HHS Public Access

Author manuscript

Nat Cardiovasc Res. Author manuscript; available in PMC 2023 May 18.

Published in final edited form as:

Nat Cardiovasc Res. 2023 April ; 2(4): 368–382. doi:10.1038/s44161-023-00254-6.

Platelet glycoprotein V spatio-temporally controls fibrin formation

Sarah Beck[1,2], **Patricia Öftering**[1,2], **Renhao Li**[3], **Katherina Hemmen**[1], **Magdolna Nagy**[4], **Yingchun Wang**[3], **Alessandro Zarpellon**[5], **Michael K. Schuhmann**[6], **Guido Stoll**[6], **Zaverio M. Ruggeri**[5], **Katrin G. Heinze**[1], **Johan W.M. Heemskerk**[4], **Wolfram Ruf**[7,8,†], **David Stegner**[1,2,†,*], **Bernhard Nieswandt**[1,2,†,*]

[1]Julius-Maximilians-Universität Würzburg, Rudolf Virchow Center for Integrative and Translational Bioimaging, Würzburg, Germany.

[2]University Hospital Würzburg, Institute of Experimental Biomedicine, Würzburg, Germany.

[3]Aflac Cancer and Blood Disorders Center, Children's Healthcare of Atlanta, Department of Pediatrics, Emory University School of Medicine; Atlanta, USA.

[4]Department of Biochemistry, CARIM, Maastricht University; Maastricht, The Netherlands.

[5]Department of Molecular Medicine, Scripps Research; La Jolla, CA, USA.

[6]University Hospital Würzburg, Department of Neurology, Würzburg, Germany.

[7]Center for Thrombosis and Hemostasis (CTH), Johannes Gutenberg University Medical Center Mainz; Mainz, Germany.

[8]Department of Immunology and Microbiology, Scripps Research; La Jolla, CA, USA.

Abstract

[*]Correspondence and requests for materials should be addressed to: bernhard.nieswandt@virchow.uni-wuerzburg.de, stegner@virchow.uni-wuerzburg.de.

[†]These authors contributed equally to this work.

Author contributions:
Conceptualization: SB, JMWH, WR, DS, BN
Methodology: YW, RL, KH, KGH, WR, BN
Investigation: SB, PÖ, MN, AZ, ZMR, JWMH, MKS, GS, DS, BN
Visualization: SB
Funding acquisition: BN, RL
Supervision: DS, BN
Writing – original draft: SB, WR, BN
Writing – review & editing: SB, PÖ, RL, KH, MKS, KGH, ZMR, JWMH, WR, DS, BN

Competing interests:
SB, DS and BN hold a patent on recombinant GPV for treating thrombotic diseases reporting soluble GPV (lacking a functional transmembrane domain) for use in the treatment or prevention of thrombotic diseases. Data on rhGPV preventing thrombus formation in vivo and reducing infarct volume in a tMCAO model in this manuscript are partly covered by the patent (patent applicant: Julius-Maximilians Universität Würzburg, Inventors: BN, DS, SB, patent published, title: soluble glycoprotein V for treating thrombotic diseases; WO 2017/109212; US Patent No. US 11,028,144 B2).
The other authors declare that they have no competing of interest.

Extended Information is available for this paper.

Code availability:
Macros used for quantitative image analysis are available at: https://github.com/HeinzeLab/GPV-flowchamber

The activation of platelets and coagulation at vascular injury sites is crucial for haemostasis but can promote thrombosis and inflammation in vascular pathologies. Here, we delineate an unexpected spatio-temporal control mechanism of thrombin activity that is platelet orchestrated and locally limits excessive fibrin formation after initial haemostatic platelet deposition. During platelet activation, the abundant platelet glycoprotein (GP) V is cleaved by thrombin. We demonstrate with genetic and pharmacological approaches that thrombin-mediated shedding of GPV does not primarily regulate platelet activation in thrombus formation, but rather has a distinct function after platelet deposition and specifically limits thrombin-dependent generation of fibrin, a crucial mediator of vascular thrombo-inflammation. Genetic or pharmacologic defects in haemostatic platelet function are unexpectedly attenuated by specific blockade of GPV shedding, indicating that the spatio-temporal control of thrombin-dependent fibrin generation also represents a potential therapeutic target to improve haemostasis.

Haemostasis is the physiological mechanism that limits bleeding after blood vessel injury through intertwined activations of circulating platelets and the plasmatic coagulation cascade[1]. The adhesion of platelets to extracellular matrix proteins and von Willebrand factor (VWF) initiates the haemostatic response that is supported by exposure of subendothelial tissue factor (TF), which triggers coagulation and local thrombin generation[2]. This results in a fibrin network encasing platelets in a stable thrombus[3]. Thrombin generation requires feed-forward reactions that involve platelet activation by thrombin-mediated cleavage and activation of G-protein coupled protease-activated receptors (PARs)[4] and amplification of coagulation reactions on the surface of activated platelets[5]. Generated thrombin forms fibrin and thereby stabilises thrombi through platelet receptor GPIIb/IIIa engagement and activates FXIII to crosslink fibrin fibres[6]. These processes are regulated with high fidelity[7] to ensure efficient haemostasis while preventing thrombosis and thrombo-inflammatory diseases[8,9]. In addition, thrombin activity in the circulation is limited by specific plasmatic coagulation inhibitors and by thrombomodulin on endothelial cells, which captures thrombin to initiate the coagulation regulatory and vascular protective protein C pathway[10].

The glycoprotein (GP) Ib-IX complex mediates platelet binding to VWF and is crucial for haemostasis. Mutations in *GP1BA*, *GP1BB* or *GP9* cause the Bernard-Soulier syndrome (BSS), a rare bleeding disorder characterised by giant platelets[11,12]. GPV is associated with the GPIb-IX complex, but not required for GPIb expression or functional interactions[13]. GPV is an abundant 88 kDa platelet/megakaryocyte-specific leucine-rich repeat (LRR) transmembrane protein[14] that interacts with collagen[15] and has minor importance for platelet function[16,17]. GPV is proteolytically cleaved by thrombin during thrombus formation[18,19], but the physiological roles of the shed 69 kDa extracellular fragment in haemostasis and thrombosis has remained elusive.

Results

Thrombus formation is accelerated in GPV mutant mice

We studied the role of GPV in thrombus formation by comparing WT and $Gp5^{-/-}$ mice in $FeCl_3$-induced thrombosis of mesenteric arterioles *in vivo*. In line with previous

observations[20], *Gp5*$^{-/-}$ mice displayed faster onset of thrombus formation and shortened occlusion times without increased embolization, indicating a prothrombotic phenotype in the absence of GPV (Fig. 1a, b). Platelet hyperreactivity to thrombin is the presumed but unproven mechanism for enhanced thrombosis in *Gp5*$^{-/-}$ mice and thought to be related to thrombin-mediated cleavage of GPV. To directly study the relevance of thrombin-mediated GPV cleavage, we generated a mouse carrying a point mutation in the thrombin cleavage site of GPV (*Gp5*^{dThr}; Extended Data Fig. 1a). Platelets of these mice showed unaltered surface expression levels of GPV compared to WT and GPV was completely resistant to cleavage by thrombin (Extended Data Fig. 1b, c, Extended Data Table 1). In contrast, cleavage of the mutant GPV by endogenous *a disintegrin and metalloproteinase* (ADAM)17[21] was not affected (Extended Data Fig. 1b–e), demonstrating the thrombin specificity of the *Gp5*^{dThr} mutation. Unexpectedly, *Gp5*^{dThr} mice displayed accelerated thrombus formation in the $FeCl_3$ arteriolar injury model, and in this respect resembled *Gp5*$^{-/-}$ mice (Fig. 1c, d).

In a series of experiments, we addressed the possibility that excessive platelet activation also caused the prothrombotic phenotype of *Gp5*^{dThr} mice. Loss of surface GPV led to hyperreactivity of *Gp5*$^{-/-}$ platelets specifically at lower thrombin concentrations but not with other agonists (Fig. 1e, g, h, Extended Data Fig. 1f–h), as previously shown[15,20,22–24]. In sharp contrast to *Gp5*$^{-/-}$ platelets, measurements of P-selectin exposure (Fig. 1f) and αIIbβ3 integrin activation and platelet aggregation (Fig. 1g, h, Extended Data Fig. 1i) showed that *Gp5*^{dThr} platelets were not hyperreactive at threshold thrombin concentration. Of note, both *Gp5*$^{-/-}$ and *Gp5*^{dThr} PRP showed unaltered clot retraction (Extended Data Fig. 1j).

We next tested the hypothesis that membrane-bound GPV might act as a regulator of thrombin-mediated PAR activation[25] supported by the GPIbα high affinity binding of thrombin[26,27]. Blockade of the GPIbα-thrombin interaction on mouse platelets with Fab-fragments of the anti-GPIbα antibody p0p/B[28,29] (Extended Data Fig. 2a) indeed diminished platelet activation, particularly at low thrombin concentrations (Extended Data Fig. 2c). Although human and mouse platelets are activated by thrombin through different PARs, these antibody inhibition data indicated that mouse platelets are similar to human platelets[25] in requiring GPIbα for thrombin-induced activation at threshold agonist concentrations. Remarkably, the anti-GPIbα antibody completely abolished the enhanced activation of *Gp5*$^{-/-}$ relative to WT platelets (Extended Data Fig. 2c), implying that loss of GPV sensitised to GPIbα-dependent thrombin signalling. In contrast, activation of *Gp5*^{dThr} platelets at threshold concentrations of thrombin was indistinguishable from WT platelets with or without anti-GPIbα p0p/B (Extended Data Fig. 2b, c). Thus, surface GPV regulates platelet responsiveness to thrombin primarily by interference with GPIbα-dependent PAR signalling in mouse platelets (Extended Data Fig. 2d, e).

The delineated pathway of enhanced *in vitro* thrombin signalling in *Gp5*$^{-/-}$ platelets could not explain the similar prothrombotic phenotype of *Gp5*$^{-/-}$ and *Gp5*^{dThr} mice *in vivo*, suggesting that shed GPV regulated thrombus formation by a mechanism unrelated to the regulation of platelet activation following vascular injury. We therefore next asked whether platelet procoagulant function might be regulated by GPV. Measurements of TF-initiated thrombin generation in platelet-rich plasma did, however, not uncover differences between

Gp5$^{-/-}$, *Gp5*^{dThr}, and WT platelets (Extended Data Fig. 2f–k), in line with previous results with GPV-deficient platelets[12], excluding alterations in platelet membrane procoagulant activity.

We next evaluated whether the known collagen interaction of GPV might contribute to the thrombus growth modulation by GPV. Platelet activation is triggered through two major signalling pathways. Specifically, soluble agonists, including thrombin and secondary mediators ADP and thromboxane A2, act through *G protein-coupled receptors* (GPCRs), whereas immobilised/multimeric ligands signal through *immunoreceptor tyrosine-based activation motif* (ITAM) coupled receptors, C-lectin like receptor 2 (CLEC-2) and GPVI. Platelet GPVI is the major activating collagen receptor and GPVI deficiency and antagonism protects from arterial thrombosis with more moderate effects on haemostasis[30]. We analysed thrombus formation in the absence or presence of platelet GPVI to uncover potential collagen binding functions of GPV. GPVI was immunodepleted from platelets by injection of the anti-GPVI antibody, JAQ1,[31] 5 days before inducing the $FeCl_3$ mesenteric arteriole injury (Extended Data Fig. 3a, b). As reported previously[31], GPVI depletion markedly attenuated occlusive thrombus formation in WT mice *in vivo*. Surprisingly, loss of GPVI was without effect in the absence of GPV and the shortened occlusion times of *Gp5*$^{-/-}$ mice persisted even after GPVI depletion in two distinct vascular beds (Extended Data Fig. 3 c–e).

In addition, GPV deficiency prevented the prolongation of the bleeding time associated with GPVI depletion in WT animals (Extended Data Fig. 3f). These data essentially excluded that GPV regulated GPVI-collagen interaction or contributed to collagen-dependent platelet activation under these experimental conditions. Rather, GPV deficiency overruled the haemostatic and thrombotic defects caused by the absence of GPVI and restored thrombus formation *in vivo*. It has previously been shown that functional defects related to GPVI-ITAM-mediated platelet activation can be attenuated by increased local thrombin generation in different vascular beds[32] and mouse GPVI does not interact with mouse fibrinogen[33]. Thus, the demonstrated reversal of GPVI inhibition in *Gp5*$^{-/-}$ mice suggested that soluble GPV (sGPV) regulated thrombin activity during thrombus formation.

sGPV binds to thrombin and localises to fibrin

We therefore evaluated the role of GPV in thrombin-mediated fibrin formation on collagen/TF spots in recalcified whole blood under flow *in vitro*[34]. Time to fibrin formation was shortened and the overall amount of fibrin generated was increased in *Gp5*$^{-/-}$ mice (Fig. 2a–c) and, importantly, also in *Gp5*^{dThr} mice (Fig. 2d–f) compared to WT controls. Quantitative imaging of formed thrombi and generated fibrin[35] showed increased thrombus height, based on multilayer and contraction scores, as well as fibrin formation, based on fibrin surface coverage and fibrin score, in the blood of both mutant mouse lines (Fig. 2g). Of note, this *ex vivo* experimental setup produced results entirely in line with the *in vivo* findings that *Gp5*$^{-/-}$ and *Gp5*^{dThr} mice concordantly displayed accelerated thrombus formation.

These data indicated that cleavage of GPV is a critical step in an autoregulatory limitation of fibrin generation. Thrombin binds to *de novo* generated fibrin via the regulatory thrombin exosites I and II and thereby becomes protected from coagulation inhibitors in the blood

[36]. We hypothesised that sGPV directly or indirectly affected thrombin-fibrin interactions. We first evaluated the direct interaction of sGPV and thrombin. We stimulated platelets with biotinylated thrombin and showed that sGPV coprecipitated in the thrombin pull down using streptavidin-coated beads (Fig. 2h), consistent with direct interaction of thrombin with sGPV.

Because GPV release was required to attenuate fibrin formation of recalcified whole blood perfused over collagen/TF spots (Fig. 2a–f), we next quantified the colocalization of GPV with fibrin in this setting. In confocal microscopy with super-resolution mode, we excluded in the image analysis platelet-rich areas based on GPIX staining and quantified subsequently the colocalization of GPV with fibrin (Fig. 2i, j, Supplementary Fig. 1). Quantification of GPV intensities showed that GPV accumulated with fibrin in platelet-free areas of thrombi (Fig. 2j).

Based on these data, we reasoned that upon initiation of a haemostatic platelet response, thrombin-mediated cleavage of GPV formed sGPV-thrombin complexes, which limited thrombin diffusion and activity in the forming fibrin clot. To test this concept, we recombinantly expressed the ectodomain of human GPV in a construct that included the thrombin cleavage site (rhGPV) (Fig. 3a). Aggregation of rhGPV at high concentrations prevented us from performing experiments with full dose response curves. However, thrombin-mediated platelet activation was only marginally inhibited by 290 nM (20 μg/ml) rhGPV at threshold thrombin concentrations (Extended Data Fig. 4a, b), in line with the conclusion that platelet activation by thrombin is primarily regulated by membrane bound GPV. In sharp contrast, rhGPV at the same concentration impaired fibrin formation in a static polymerization assay (Fig. 3b, Extended Data Fig. 4c, d) triggered specifically by thrombin, whereas fibrin polymerization induced by another protease, batroxobin, was unaltered in the presence of rhGPV (Fig. 3b, Extended Data Fig. 4c, d). Importantly, sGPV localized to fibrin polymers independent of the clot inducing enzyme, indicating direct interactions of GPV with fibrin independent of thrombin-GPV complex formation.

These data also indicated that sGPV in the developing clot directly inhibited thrombin's activity to form fibrin. We therefore studied the interaction of rhGPV with thrombin in the absence of fibrinogen. Incubation of equimolar concentrations of thrombin with rhGPV containing the thrombin cleavage site resulted in time dependent rhGPV proteolysis, demonstrating that GPV is a thrombin substrate independent of anchoring to the platelet surface (Extended Data Fig. 4e–g). However, formation of sGPV stopped after 5–10 minutes when approximately 50% of the substrate was consumed. Measurements of thrombin activity towards a chromogenic substrate was unchanged during the reaction time, excluding instability of the enzyme (Extended Data Fig.4g). Of note, at the end of the incubation time, sGPV still inhibited thrombin's activity to form fibrin (Extended Data Fig. 4h–j). To distinguish between substrate depletion and product inhibition, we performed the same reaction with a 10-fold higher substrate concentration. This reaction yielded essentially the same amount of product, implying that the generated sGPV caused product inhibition and interacted with thrombin independent of fibrin binding. Attempts to chemically crosslink sGPV and thrombin under these conditions were unsuccessful, suggesting that the required amino groups were not in close enough proximity.

rhGPV reduces fibrin formation and protects from thrombosis

In addition, rhGPV impaired fibrin formation in human (Extended Data Fig. 5a–c) and mouse blood (Extended Data Fig. 5d–g) in the collagen/TF-induced thrombus formation assay under flow, supporting a role for sGPV in limiting thrombin activity towards fibrin. Analysis of the formed fibrin fibrils by confocal microscopy revealed a fine, dense, and branched network consisting of thin, clearly distinguishable fibres in control samples, whereas fibres were generally thicker, but less frequently and structurally less defined in the presence of rhGPV (Extended Data Fig. 5f), confirming that rhGPV impedes fibrin formation. Of note, a His-tagged fusion protein did not reduce fibrin formation, demonstrating specificity of the recombinant GPV.

We next measured thrombin activity in the outflow of the flow chamber and found that less thrombin activity was recovered in rhGPV-treated samples compared to controls (Extended Data Fig. 5h). Conversely, we found more thrombin in the outflow of the chambers perfused with $Gp5^{-/-}$ and $Gp5^{dThr}$ versus WT blood (Extended Data Fig. 8a), further supporting the conclusion that sGPV controlled thrombin activity specifically in fibrin clots. We next imaged thrombin activity in flow chambers cleared of blood by perfusion with Tyrode's buffer and thrombin substrate Z-GGR-AMC. We found reduced thrombin activity in clots formed in the presence of rhGPV (Extended Data Fig. 5i, j). Taken together, these data support a role for GPV in retaining thrombin in fibrin clots and limiting thrombin's activity in fibrin formation.

We next tested whether rhGPV could modulate thrombus formation *in vivo*. Indeed, a single intravenous dose of 20 μg rhGPV prior to thrombosis induction reduced arterial thrombus formation in two different experimental models. In a model of mechanical injury to the abdominal aorta where blood flow and occlusive thrombus formation was monitored by an ultrasonic flow probe (Fig. 3c, Extended Data Fig. 5k), 14/15 mice did not form stable thrombi after rhGPV administration within the observation period of 30 minutes, whereas 18/18 arteries occluded in the control group. In $FeCl_3$-induced mesenteric arteriole injury, time to occlusion was markedly prolonged in mice treated with rhGPV (Fig. 3d, e).

In addition, rhGPV treatment provided protection from thrombo-inflammatory neurological damage and improved neurological outcome in the transient middle cerebral artery occlusion (tMCAO) model of ischaemic stroke (Fig. 3f–h) in which the concerted action of platelets, the coagulation system and immune cells is known to drive post-ischaemic cerebral infarct growth[37]. Of note, infarct volumes of $Gp5^{-/-}$ and $Gp5^{dThr}$ mice after tMCAO were comparable to WT mice (Fig. 3f–g), suggesting that thrombin activity in WT mice is already above threshold values needed to fully promote infarct progression under these experimental conditions. Importantly, no large intracranial haemorrhages were observed in $Gp5^{-/-}$ or $Gp5^{dThr}$ and rhGPV-treated WT mice (Fig. 3g). Of note, MCA vessel diameters were similar in $Gp5^{-/-}$ and WT mice (Extended Data Fig. 6). In addition, haemostatic function evaluated by tail bleeding time assay was also comparable between rhGPV-injected mice and vehicle-treated controls (Fig. 3i), indicating that this pathway might be targeted safely. Together, these data showed that sGPV specifically limited fibrin formation and pathological intravascular thrombus growth without impairing initial platelet activation required for haemostasis.

Blocking GPV cleavage offsets defects in haemostatic platelet function

To further study thrombin interaction with GPV, we generated a panel of anti-GPV monoclonal antibodies (termed DOM mAbs; Extended Data Fig. 7) and first evaluated their ability to inhibit thrombin mediated GPV cleavage (Fig. 4a). Cleavage of substrates by thrombin involves binding and allosteric regulation by thrombin exosites I and II that flank the active site[38]. Blockage of exosite I with the thrombin binding aptamer HD1[39] was more efficient than blocking exosite II with HD22[40], whereas a non-blocking aptamer HD23 was without effect on thrombin-mediated release of GPV from platelets (Extended Data Fig. 7g). Thus, thrombin interaction with fibrin and GPV occurred through overlapping sites[36]. With this screening assay, we identified mAb DOM/B that markedly reduced thrombin-mediated GPV cleavage and synergised with thrombin exosite-directed aptamers (Fig. 4a, S8g), whereas mAb DOM3 was non-inhibitory (Fig. 4a, f, Extended Data Fig. 7b). In platelet-rich plasma, we tested inhibitory activities of DOM/B in a thrombin-induced clotting assay, in which fibrin is formed independent of platelet activation. Whereas thrombin exosite II blockade with HD22 prolonged clotting times, clotting was unaffected by DOM/B-treatment as well as was indistinguishable between WT, $Gp5^{-/-}$ and $Gp5^{dThr}$ samples (Extended Data Fig. 7h). Thus, thrombin regulation by GPV specifically occurs under conditions of platelet activation under flow.

In addition, DOM/B had no effect on thrombin-induced platelet activation (Extended Data Fig. 7d–f), indicating that this mAb did not sterically hinder the interaction of GPV with the GPIb-IX complex involved in GPIbα-thrombin-PAR platelet signalling. Remarkably, however, DOM/B significantly shortened time to fibrin formation and increased the amount of generated fibrin under flow conditions (Fig. 4b, c) as well as the thrombin activity in the outflow of the flow chamber (Extended Data Fig. 8a), thereby reproducing the phenotypes seen with $Gp5^{-/-}$ and $Gp5^{dThr}$ mice. In line with reduced proteolytic release of GPV in the presence of DOM/B, we found less GPV colocalizing with fibrin compared to controls (Extended Data Fig. 8b). The panel of anti-GPV mAbs was also evaluated for interference with collagen-dependent platelet activation. Whereas DOM/B and DOM3 were non-inhibitory (Extended Data Fig. 7b, c), inhibition of platelet activation in this assay by DOM/C indicated that this mAb was directed against the collagen binding site of GPV (Extended Data Fig. 7a). DOM/C did not interfere with thrombin mediated GPV cleavage (Fig. 4a), and did not enhance fibrin formation under flow, consistent with the crucial and specific role of sGPV release in this context (Fig. 4d, e). This data suggested that the collagen binding activity of (s)GPV is functionally not required for its ability to modulate fibrin formation under flow *in vitro* and *in vivo*.

We next evaluated the effect of blocking GPV-thrombin interaction with DOM/B on fibrin and thrombus formation *in vivo*. Of note, injection of DOM/B did not cause platelet depletion and the mAb remained detectable on the surface of circulating platelets for up to 6 days (Extended Data Fig. 8c, d). In line with the observed increased fibrin formation under flow *in vitro*, DOM/B treatment caused accelerated thrombus formation in $FeCl_3$-injured mesenteric arterioles *in vivo*, whereas neither blockade of the collagen binding site on GPV with DOM/C nor the non-inhibitory DOM3 affected thrombus formation (Fig. 4f, g). These data showed that the release of sGPV acts as a safety valve to limit thrombus

growth after initial platelet activation required for haemostasis. We have previously shown that the absence of the two major collagen receptors GPVI and integrin α2β1 causes severe bleeding in mice[41]. In line with the reversal of bleeding defects caused by GPVI-deficiency in *Gp5*$^{-/-}$ mice, DOM/B-treatment restored haemostasis and thrombus formation in the complete absence of the two major platelet collagen receptors GPVI and α2β1 (Extended Data Fig. 8e–g, summarized in Extended Data Fig. 8h).

These results suggested that interference with GPV cleavage can be utilised to enhance fibrin formation in the context of defective haemostasis caused by diverse mechanisms. We therefore investigated whether GPV cleavage blockade with DOM/B not only restored haemostasis in the case of defective (hem)ITAM signalling, but also other genetic and pharmacological impairments of platelet function. Lack of the small GTPase RhoA causes macrothrombocytopenia and defective platelet activation, resulting in a bleeding defect[42]. Similarly, Nbeal2-deficiency leads to macrothrombocytopenia and lack of α-granules resulting in severely impaired haemostasis[43]. Interestingly, DOM/B-treatment improved and restored haemostasis in mice with platelet RhoA deficiency or lacking Nbeal2 (Fig. 4h, i).

Thrombocytopenia is a major clinical challenge occurring frequently in the context of a variety of pathologies or medical treatments that is associated with increased bleeding and often with the need of immediate therapeutic intervention[44,45]. To test a possible benefit of a GPV cleavage blockade in this setting, we induced severe thrombocytopenia by reducing platelet counts to 5–10% of normal by injecting a platelet-depleting antibody[46,47]. While a resulting severe bleeding defect was observed in all 9 platelet-depleted control mice, this was significantly attenuated by DOM/B-treatment, and remarkably 9/11 DOM/B-treated thrombocytopenic mice managed to stop bleeding within the observation period (Fig. 4j). The current clinical standard of care to reduce the risk of heart attack and ischaemic stroke is the pharmacological inhibition of platelet function by $P2Y_{12}$ ADP receptor blockers alone or in combination with acetyl salicylic acid (ASA). As seen in humans, mice treated with the $P2Y_{12}$-blocker clopidogrel exhibit increased bleeding that was reversed by treatment with DOM/B blocking thrombin-dependent GPV release from platelets (Fig. 4k). Thus, specific targeting of GPV with DOM/B prevented the prolongation of the bleeding time caused by thrombocytopenia, genetic defects, and anti-platelet therapy, indicating clinical potential of anti-GPV treatment to restore haemostasis by improving thrombin-dependent fibrin formation.

Blocking GPV cleavage increases fibrin formation in human blood

We therefore evaluated the relevance of this concept for human platelet function and screened a panel of newly generated anti-hGPV mAbs (termed LUM mAbs) for their ability to interfere with thrombin-mediated cleavage of GPV. Recapitulating the inhibitory properties of DOM/B in the mouse system, LUM/B prevented thrombin-mediated cleavage of GPV on human platelets, whereas other anti-hGPV mAbs (LUM1–5) were non-inhibitory (Fig. 5a and Extended Data Fig. 9c). LUM/B per se neither activated human platelets (Fig. S10a, b) nor influenced thrombin clotting (Extended Data Fig. 9e) nor thrombin-induced platelet activation as shown by unaltered integrin αIIbβ3 activation or P-selectin exposure in the presence of the antibody (Fig. 5b, Extended Data Fig. 9d). In the established

flow assay on immobilised collagen/TF, GPV blockage on human platelets with LUM/B significantly accelerated fibrin formation in recalcified whole blood (Fig. 5c–e), whereas the non-inhibitory LUM3 was without effect (Extended Data Fig. 9f, g). Thus, spatio-temporal control of fibrin formation on thrombogenic surfaces by GPV is a species-conserved mechanism to restrict thrombosis while preserving haemostasis.

Discussion

We here delineate the function of platelet GPV that is proteolytically released by thrombin in the context of platelet activation at sites of vascular injury. Genetic blockade of thrombin-mediated shedding of GPV uncovered the crucial role of sGPV as a regulator of fibrin formation and thrombus growth. The cleavage of membrane bound GPV occurs after platelet adhesion and initiation of thrombin generation and is thus temporally separated from the initial haemostatic response. We show that generated sGPV then interacts with generated fibrin and dampens thrombin activity towards fibrinogen. This spatially restricted action of sGPV after release from the platelet surface specifically limits thrombus growth in vitro and in vivo (summarized in Fig. 6). As demonstrated by pharmacological application of rhGPV, sGPV provides protection from thrombo-inflammatory neurological damage in an experimental model of ischemic stroke without causing haemostatic impairments. Conversely, specific blockade of thrombin mediated GPV shedding can enhance local fibrin formation in a variety of contexts associated with severe defects in platelet function. This unique spatio-temporal control of thrombin activity by GPV can thus be harnessed to promote haemostasis.

Prevention of thrombosis while preserving haemostasis has been a central goal of antithrombotic drug development. Despite the broader application and safety of target selective oral anticoagulants, preventing bleeding complications remains an unmet clinical need. Although a recent study provides proof of principle that platelet mediated thrombin generation can rescue bleeding defects due to increased fibrinolysis[47], there is an unmet clinical need for more general and specific spatio-temporal control of fibrin formation. Novel haemostatic agents are approved or in development to bypass genetic or acquired deficiencies in the coagulation cascade[48], but platelet transfusion remains the only therapeutic option to acutely restore defective platelet function or severe forms of thrombocytopenia to secure haemostasis. Akin to the strategies that ‘inhibit the inhibitors’ of coagulation, we here propose a therapeutic strategy of tailored activation of haemostatic fibrin plug formation in the spatio-temporal context of platelet deposition at sites of vessel wall injury. By increasing local thrombin bioavailability without compromising scavenging of thrombin by endothelial cell-expressed thrombomodulin, this approach has little risk to interfere with physiological anticoagulation in the body and vascular protective and anti-inflammatory signalling of the protein C-PAR1 pathway[10].

Methods

Animals

Mice were maintained under specific pathogen-free conditions (constant temperature of 20–24°C and 45–65% humidity with a 12-h light–dark cycle, ad libitum water and food access)

and experiments were performed in accordance with German law and the governmental bodies, and with approval from the District of Lower Franconia.

Gp5$^{-/-}$[12] and *Itga2*$^{-/-}$[49] mice were kindly provided by François Lanza (Inserm-Université de Strasbourg, Strasbourg, France) and Beate Eckes (Department of Dermatology, University of Cologne, Cologne, Germany), respectively. *Gp5*^{dThr} mice, which carry a point mutation in the thrombin cleavage site of GPV, were generated are described in Extended Data Figure 1A). *Gp5*^{dThr} mice were intercrossed with Flip-positive mice to delete the Neo-cassette and backcrossed to C57Bl/6J background. *RhoA*$^{fl/fl}$[50] mice were kindly provided by Cord Brakebusch (University of Copenhagen, Copenhagen, Denmark). To generate MK-/platelet-specific knockout mice, the floxed mice were intercrossed with mice carrying the Cre recombinase under control of the Pf4 (platelet factor) promoter. *Nbeal2*$^{-/-}$[43] mice were described previously. All mice were kept on a C57Bl/6J background and all animal experiments and the analysis of the corresponding data were performed blinded.

Female Wistar rats (strain: RjHan:WI, starting at 6 weeks of age) were immunized to generate monoclonal anti-GPV antibodies.

Human blood samples

For this study, blood samples were obtained from healthy volunteers, free from anticoagulant or anti-platelet therapy for at least 4 weeks, following written informed consent in accordance with the Declaration of Helsinki and after approval by the Institutional Review Boards (IRB) of University of Würzburg (votes 167/17 and 295/20).

Chemicals

Midazolam (Roche Pharma AG), dorbene (Pfizer) and fentanyl (Janssen-Cilag GmbH) were used according to regulations of the local authorities. Clopidogrel was from Sanofi, low-molecular-weight heparin from ratiopharm GmbH and recombinant hirudin from Coachrom. Human fibrinogen (#F4883), bovine thrombin (T4648), N-ethylmaleimide (NEM, 23030) and Prostacyclin (PGI_2) were from Sigma-Aldrich. Prolong Glass antifade mountant (P36980) and fibrin(ogen) AF488 (F13191) were from Thermo Scientific. Iron(III)chloride ($FeCl_3$) was from Roth. A23187 was from AppliChem, ionomycin from VWR. Convulxin was from Axxora. Fibrillar type I collagen (Horm) was from Takeda, Rhodocytin was provided by Johannes Eble (University of Münster, Münster, Germany). Collagen-related peptide (CRP) was generated in-house by formaldehyde-cross-linking of $GKO(GPO)_{10}GKOG$ (purchased from Cambridge Research Biochemicals, with O = L-hydroxyproline) [51]. Integrilin was from GlaxoSmithKline. Human thrombin was from Roche (Sigma-Aldrich #10602400001). Apyrase type III was from GE Healthcare, biotinylated thrombin (69672–3) was from Merck/Millipore. Z-GGR-AMC-HCl was from Bachem, thrombin calibrator was from Stago, human recombinant tissue factor (Dade Innovin) was from Siemens Healthcare. Fluorogenic thrombin substrate Pefafluor TH was from Pentapharm. Donkey anti-rat IgG FITC (#112095068) was from Jackson Immuno Research (West Grove, PA, USA). DNA aptamers (HD1: GGT TGG TGT GGT TGG, HD22: AGTCCGTGGTAGGGCAGGTTGGGGTGACT) to block thrombin exosites and

control aptamer HD23 (AGTCCGTAATAAAGCAGGTTAAAAT GACT) were from Future Synthesis (Poznań, Poland).

Antibodies

PAC-1-FITC (#340507) and anti-CD62P-APC (#550888) antibodies were from BD Biosciences, control rat IgG (#I4131) and anti-GAPDH (#G9545) were from Sigma. Anti-mGPV antibody (#AF6990) for Western blot analysis was from R&D, the anti-hGPV antibody (#sc271662) for Western blot analysis from Santa Cruz. The platelet-depletion antibody R300 (rat anti-GPIbα IgG antibody) was from Emfret Analytics (Eibelstadt, Germany). Anti-mCD31 (clone: 390, in-house conjugated to AF647) was from BioLegend (#102402). A detailed list of in-house generated antibodies is provided in the supplementary information (Supplementary Table 1). The novel antibodies were generated by hybridoma technology following immunisation of *Gp5*$^{-/-}$ mice or Wistar rats with recombinant hGPV protein or GPV immunoprecipitated from mouse or human platelet lysates.

Expression and purification of recombinant hGPV

The gene fragment encoding the GP64 signal peptide (MVSAIVLYVLLAAAAHSAFA), human GPV extracellular domain (aa 17–518), and a decahistidine tag was amplified, inserted into pFastBac™ dual vector and transformed into DH10Bac *E. coli* strain (ThermoFisher Scientific). The resulting bacmid DNA was prepared and then transfected into Sf9 insect cells (ThermoFisher Scientific, #11496015) using cellFectin II reagent (ThermoFisher). The high-titer P2 baculovirus stock was prepared from scaled-up Sf9 cells in Sf-900 II serum-free media (ThermoFisher Scientific, #10902088) following the instruction of Bac-to-Bac™ Baculovirus Expression System (ThermoFisher Scientific) and used to induce hGPV expression in Sf9 cells (2×10^6 cells/ml, MOI 2) for 72 hours. hGPV was purified from insect cell media by Ni-affinity chromatography using a GE Healthcare Ni Sepharose excel column (elution buffer: 20 mM sodium phosphate, 500 mM NaCl, 500 mM imidazole, pH 7.4), followed by size exclusion chromatography using a GE Healthcare HiLoad 16/600 Superdex 200 pg column (elution buffer: phosphate buffered saline (PBS) containing 0.1% tween20, pH 7.4). The purified protein was stored at −80°C in PBS containing 0.1% tween20 and 20% glycerol. Notably, rhGPV precipitated at concentrations above 0.5 mg/ml limiting its biophysical characterization.

Antibody treatment

For the antibody treatment experiments the mice were separated into antibody and control treatment group in a randomized manner using https://www.random.org/lists/. 100 μg JAQ1 IgG were injected intraperitoneally at day 7 and day 5 prior to the experiment, resulting in a GPVI knockout like phenotype[31]. All other antibodies (each 100 μg) were injected i.v. or i.p. directly before the experiment.

Platelet depletion

Thrombocytopenia was induced by intravenous injection of rat anti-GPIbα IgG antibody R300 (Emfret Analytics, Eibelstadt, Germany, 0.14–0.18 μg/g body weight). This low dose of platelet depletion antibody reduced the platelet count to 5–10% of the initial platelet

count[46]. Peripheral platelet count was determined by flow cytometry 16 h after platelet depletion (prior to tail bleeding time experiment).

Treatment with clopidogrel or rhGPV

Mice were fed orally with 3 mg/kg clopidogrel 48 h and 24 h before the experiment. A dose titration for rhGPV was performed using 10–80 μg rhGPV per mouse in an arterial thrombosis model. 10 μg rhGPV resulted in variable results, while no difference in the anti-thrombotic effect of rhGPV was noted for 20, 40 or 80 μg rhGPV/mouse. Consequently, 20 μg (as the lowest rhGPV-concentration that yielded reproducible results) were chosen for all *in vivo* experiments and 20 μg/ml for *in vitro* assays. Mice were injected intravenously with 20 μg rhGPV 5 min before the experiment.

Preparation of PRP and washed platelets

Mice were anesthetised using isoflurane and bled to 300 μl heparin (20 U/ml in TBS, pH 7.3, Ratiopharm). The blood was centrifuged twice at 300 g for 6 min to obtain platelet-rich plasma (PRP). PRP was supplemented with 0.02 U/ml apyrase (A610, Sigma-Aldrich) and 0.1 μg/ml PGI_2 (P6188, Sigma-Aldrich) and platelets were pelleted by centrifugation at 800 g for 5 min, washed twice with Tyrode's buffer (134 mM NaCl, 0.34 mM Na_2HPO_4, 2.9 mM KCl, 12 mM $NaHCO_3$, 5 mM HEPES, 5 mM glucose, 0.35% BSA, pH7.4) containing 0.02 U/ml apyrase and 0.1 μg/ml PGI_2. The platelets were allowed to rest for at least 30 min at 37°C prior to experiments.

Aggregation assay

Washed platelets (160 μl with 1.5×10^5 platelets/μl) and PRP (only used for ADP stimulation) were prepared as described. For aggregometry, washed platelets were analysed in the absence (thrombin) or presence (all other agonists) of 70 μg/ml human fibrinogen. Antibodies (10 μg/ml) were preincubated for 5 min at 37°C prior to the experiment. Light transmission was recorded on a four-channel aggregometer (Fibrintimer; APACT, Hamburg, Germany) for 10 min or 20 min (in the presence of LEN/B) and expressed in arbitrary units, with buffer representing 100% light transmission. Platelet aggregation was induced by addition of the indicated agonists.

Flow cytometry

To determine glycoprotein surface expression levels, whole blood was diluted 1:20 with Ca^{2+}-free Tyrode's buffer or PBS and stained with saturating amounts of fluorophore-conjugated antibodies for 15 min at RT in the dark.

Washed platelets adjusted to 50000/μl in Tyrode's buffer with Ca^{2+} were stimulated with the indicated agonists and incubated with saturating amounts of fluorophore-conjugated antibodies to determine platelet activation or thrombin-mediated cleavage of GPV. Human Thrombin (Sigma #10602400001) was used to stimulate platelets.

All samples were analysed directly after addition of 500 μl PBS on a FACSCalibur (BD Biosciences, Heidelberg, Germany) using the CellQuestPro (v6.0) software. Data were analysed using FlowJo (v10.7 and v10.8.1). An exemplified gating strategy based on

FSC/SSC characteristics is provided in the supplementary information (Supplemental Figure 2).

Thrombin- and NEM-induced cleavage of GPV

Washed platelets were adjusted to a concentration of 1×10^6 platelets/µl in Tyrode's buffer without Ca^{2+} and diluted 1:1 with Tyrode's buffer without Ca^{2+} (for resting and thrombin-stimulated samples (human Thrombin (Sigma #10602400001)) and with Tyrode's buffer with Ca^{2+} (for NEM (2 mM f.c.)-incubated samples). Stimulation with 867 pM thrombin (human thrombin: 0.1 U/ml is equivalent for 867 pM thrombin) for 30 min at 37°C was performed in the presence of 40 µg/ml integrilin and 5 µM EGTA to prevent platelet aggregation. Afterwards, platelet suspension was diluted and incubated with saturating amounts of FITC-conjugated platelet surface antibodies and were directly analysed on a FACSCalibur. The residual platelet suspension was pelleted, and the supernatant analysed in a GPV ELISA.

GPV ELISA

96-well plates (Hartenstein, Würzburg, Germany, F-Form) were coated with 50 µl/well DOM/C antibody (30 µg/ml) in carbonate buffer o/n at 4°C, blocked with 5% non-fat dried milk in PBS for 2 h at 37°C and washed. Samples were applied to plates, incubated for 1 h at 37°C and washed. Plates were incubated with HRP-labelled DOM/B antibody for 1 h, washed again 3 times and developed using TMB substrate. The reaction was stopped by addition of 0.5 M H_2SO_4. Optical density was measured on a Multiskan Ex device (Thermo Electron Corporation, Braunschweig, Germany). Absorbance was read at 450 nm, the 620 nm filter served as reference wavelength. Plasma samples from *Gp5*$^{-/-}$ mice served as negative control, supernatant after platelet thrombin stimulation as positive control.

Clot retraction

Clot retraction studies were performed at 37°C in an aggregometer tube containing diluted PRP (3×10^5 platelets/µl), thrombin (34.68 nM), and $CaCl_2$ (20 mM). Clot retraction was recorded with a camera over a time span of 2 h after activation.

Thrombin time

To determine thrombin time, citrated PRP was diluted 1:1 in PBS and stimulated with 17.5 nM f.c. bovine thrombin (equivalent to 2 U/ml). Thrombin time was analysed with a 4-channel mechanical ball coagulometer (Merlin medical, Lemgo, Germany).

Thrombin generation

Thrombin generation was quantified in recalcified citrate-anticoagulated PRP with platelet count adjusted to 1.5×10^5 platelets/µl. Platelets were resuspended in pooled plasma preparations from 2–4 mice with the same genotype. After platelet stimulation with the indicated agonists (15 min at 37°C), samples in duplicates (4 vol) were transferred to a polystyrene 96-Immulon 2HB well plate. The wells either contained 1 vol thrombin calibrator or tissue factor (1 pM f.c.). Coagulation was initiated by adding 1 vol of fluorescent thrombin substrate (2.5 mM Z-GGR-AMC). Thrombin generation was measured

and analysed using the Thrombinoscope™ software (version 5.0.0.742, ThrombinoscopeBV, Maastricht, The Netherlands).[52,53]

Static fibrin polymerisation

Unlabelled fibrinogen (1.35 mg/ml f.c.) and Alexa Fluor A488-labelled fibrinogen (45 μg/ml f.c.) were mixed (30:1) in the absence or presence of rhGPV (20 μg/ml, stained with LUM/B AF647). Fibrin polymerisation was initiated by addition of 867 pM thrombin or 1 U/ml batroxobin (Loxo, Dossenheim, Germany) in the presence of 5 mM $CaCl_2$. The mixture was immediately transferred to an uncoated 15μ-slide 8-well (Ibidi GmbH, Gräfelfing, Germany), and placed in a dark humidity chamber for 2 h at room temperature to allow fibrin polymerisation. Images were obtained using a Leica SP8 inverted microscope with a 63x oil immersion lens. Optical z-stacks (8 μm, 0.1 step size, Nyquist conform) were deconvolved (Huygens Essential Software, v21.04) and are shown as maximum projection (Image J software). Fibrin fibres per visual field and surface coverage of hGPV staining were quantified using Fiji.

Coagulation flow chamber

Glass coverslips were coated with collagen type I (10 μl, 50 μg/ml) and tissue factor (TF; 10 μl, 100 pM or 10 pM for experiments with human blood or mouse blood, respectively) and blocked with 1% BSA/PBS. Citrated whole blood was recalcified by co-infusion with 6.3 mM $CaCl_2$ (f.c.) and 3.2 mM $MgCl_2$ (f.c.) and perfused over the collagen/TF spots for up to 6 min at a shear rate of 1000 s^{-1} [54]. Before each experiment, blood samples were pre-labeled with Alexa Fluor™ (AF) 488-conjugated fibrinogen, an anti-GPIX derivative (mouse) or anti-GPIbβ derivative (human) to stain platelets. For human samples, control and antibody-treated samples of the same donor were always run in parallel.

1. **Time series experiments:** Before each experiment, blood samples were preincubated with AF488-conjugated fibrinogen, AF647-conjugated anti-GPIX derivative (mouse) or AF647-conjugated anti-GPIbβ derivative (human) platelets. For time series experiments, fluorescence microscopic images were captured at 30 s intervals, to evaluate kinetics for up to 6 min (Leica DMI 6000 B, 63x objective, Leica Application Suite (LAS) X software (version 1.9.013747)). Recorded images were further processed with the background subtraction method ICC (Instant Computational Clearing) to remove out-of-focus blur on a Leica Thunder microscope (LASX software v3.7). Next, the exported images were analysed for surface area coverage of fibrin formation with self-written Python scripts[55]. In detail, in the first step an entropy filter with a disk size of 5 pixel was applied, followed by a median filter (disk size 10 pixel) and Otsu-thresholding. To compensate for a nearly empty field of view during the first images in the time series, we introduced a "scaling factor" *sf* with which we multiplied the found Otsu-threshold value, and thus increased the threshold slightly for the first images (usually the first 60–150 s, with $sf = 1.03 – 1.05$). The thresholded area (as fraction of the whole field of view) represents the area covered by fibrin.

For heatmap representation, mean values were univariate scaled from −4 to 4. Gene effect heatmaps were constructed by subtracting scaled average values of the control strain from the mutant strain. For details see[35].

2. 3D confocal microscopy—Samples were stained as described for 1. Time series experiments. To acquire z-stacks of complete thrombi, samples were fixed with 4% PFA/PBS, mounted with Prolong Glass (Thermo Scientific) and further analysed by confocal microscopy (Leica SP8 inverted microscope). Z-stack of thrombi were acquired at a SP8 confocal microscope (Leica) Hyvolution mode, 63x, z-step: 0.1 µm. Images were deconvolved using Huygens Professional Software (v 21.04) with a signal-to-noise ratio (SNR) between 2–10 (identical for regions of interest in the same animal), an automatic background subtraction using the in/near object option with a search radius of 2 µm, and maximal 40 iterations. The deconvolved data set was exported as Imaris file format and visualised with Fiji[56] (https://www.biovoxxel.de/development/).

To analyse GPV-fibrin localisation outside the thrombus, blood samples were preincubated with AF488-conjugated fibrinogen, AF546-conjugated anti-GPV derivative (as direct labelling of rhGPV with a fluorophore abolished its biological activity) and AF405-conjugated anti-GPIX derivative. Single images from the bottom of a thrombus were acquired using a Zeiss LSM 980 Airyscan microscope (63x objective) in superresolution mode using the smart setup. Images were deconvolved by Zeiss ZEN software (v3.2) and analysed with Fiji. First, masks from the fibrin(ogen) and platelet (GPIX) channel were generated using Li thresholding. Masks were then used as “positive” (pixel intensity = 1 inside structure and = 0 outside the structure) and “negative” imprints (pixel intensity = 0 inside the structure and = 1 outside the structure) and applied to the GPV channel. To analyse GPV intensities outside thrombus but inside fibrin fibres, the positive fibrin mask is multiplied with the negative thrombus mask.

In detail, after Li thresholding the intensity values in the binarized images were changed to 0 and 1 by dividing through 255. Next, this procedure for preparation of the positive and negative binary mask was repeated for the GPIX channel. Afterwards, the prepared masks based on single-cannel thresholds were combined by multiplication (leading to a value of 1, if positive in both masks). This resulted in the following regions:

- Inside fibrin but non-platelet area
- Outside fibrin & non-platelet area => background count rate

Finally, the intensity of GPV was determined in the area of fibrin by multiplication of the obtained masks with GPV channel. Values outside the mask were set to 0, pixel inside the mask have an intensity of 1, thus the original intensity of GPV was preserved. This calculation was performed for all masks and surface coverage as well as raw integrated density were determined. Then, the average intensity per pixel was calculated inside the covered area and the raw integrated density was divided by the number of pixels to obtain the average intensity per non-zero pixel.

For each step, a Fiji macro was recorded. All Fiji macros and Python scripts used for the fluorescence image analysis can be downloaded from: https:\\github.com\HeinzeLab\GPV-flowchamber

Thrombin activity

Coagulation flow assay was performed as described above without staining for platelets and fibrin(ogen). The outflow was collected in 10 mM EDTA and 1.5 μM HD1. Thrombin activity was measured immediately using the fluorogenic thrombin substrate Pefafluor TH (Pentapharm) at 460 nm.

Thrombin activity in the formed thrombi was determined using the fluorogenic thrombin substrate Z-GGR-AMC.

Western Blot after pulldown

Washed platelets were adjusted to 1×10^6 platelets/μl and either left unstimulated or were stimulated with biotinylated thrombin (433 pM) for 15 min at 37°C. Where indicated, Hirudin (0.1 U/ml) or GM6001 (100 μM f.c.) were added before platelet stimulation. Platelets were pelleted and the supernatant was incubated with magnetic Streptavidin beads to pulldown biotinylated thrombin. After incubation, beads were collected and washed. The eluate was used for Western blot analysis and the samples were detected with an anti-GPV antibody (R&D).

GPV-thrombin interaction in solution

We performed cross-linking experiments with BS3 or DTSSP following incubation of thrombin with varying concentrations of rhGPV. However, conditions with efficient cross-linking could not be established. Thrombin interaction with rhGPV was furthermore analyzed in a solution (Hepes buffer) and generation of sGPV was followed by Western blotting and detected with an anti-hGPV antibody (Santa Cruz, sc271662). A serial dilution of cleaved sGPV was used to quantify the reaction product. The stability of thrombin was analysed under the same conditions by determining thrombin activity with the chromogenic substrate S2238 (Chromogenix).

Tail bleeding time

Mice were anaesthetised by intraperitoneal injection of triple anaesthesia (Dormitor 0.5 μg/g, Midazolam 5 μg/g, and Fentanyl 0.05 μg/g body weight) and a 1-mm segment of the tail tip was removed using a scalpel. Tail bleeding was monitored by gently absorbing blood on filter paper at 20 s intervals without directly contacting the wound site. When no blood was observed on the paper, bleeding was determined to have ceased. The experiment was manually stopped after 20 min by cauterization.

Light sheet fluorescence microscopy (LSFM)

Sample preparation—The vasculature was stained by intravenous injection of AF647-conjugated anti-CD105 (clone MJ7/19, purified in-house, 0.4 μg $^{-1}$) and AF647-conjugated anti-CD31 (BioLegend, clone 390, 0.4 μg g^{-1}). 30 min after in vivo labeling mice were

anesthetized by intraperitoneal injection of medetomidine 0.5 μg/g, midazolam 5 μg/g and fentanyl 0.05 μg/g body weight and transcardially perfused with ice-cold PBS to wash out the blood and ice-cold 4% paraformaldehyde (PFA, P6148, Sigma-Aldrich, Germany, pH 7.2). Brains were removed, washed in PBS and dehydrated in methanol solutions of increasing concentrations (50%, 70%, 95%, 100%) to fix the tissue. The methanol was replaced stepwise by a clearing solution consisting of one part benzyl alcohol to two parts benzyl benzoate (BABB, catalog nos. 305197 and B6630, Sigma-Aldrich). After incubation in the clearing solution for at least 2 h at RT, tissue specimens became optically transparent and were used for LSFM imaging on the following day.[57]

Optically cleared brains were imaged with a custom-build light sheet microscope equipped with two EC Epiplan. Neofluar 2.5x/0.06 M27 excitation objectives (Zeiss, Germany) and a HCX FLUOTAR 5x/0.15 Dry detection objective (Leica, Germany)[29] with a voxel size of 2.6 μm and a z-spacing of 5 μm (Pixel size: 2.6×2.6×5 μm). Major parts of the LSFM have been described previously[58]. Additionally, to the fluorescence signal of the AF647-conjugated antibodies staining the vessel system also the brain autofluorescence was collected by excitation at 488 nm / emission 520 nm.

Segmentation of brain LSFM images

Images acquired by LSFM were saved in TIFF format and converted to the Imaris file format (Imaris 9.9, Bitplane, Oxford) for further processing and segmentation. Using the built-in image processing tools, first the background was subtracted from both channels and secondly a 3×3×3 voxel median filter was applied to the vessel channel (AF647 fluorescence). Next, the median filtered vessel channel was segmented using the surface tool. Here, a four-voxel smoothing (10.4 μm) and a local contrast intensity thresholding (10 μm diameter) was applied. The intensity threshold was adjusted manually to ~ 50 % of the automatically proposed value. Finally, objects smaller than 1000 voxel were removed.

Determination of vessel diameter

To determine the diameter of the vessel at selected regions of interest, the generated vessel surface was masked onto the vessel fluorescence such that the intensity outside the surface was zero while inside the surface the original, median filtered intensity values are present.

To estimate the diameter, the measurement points option in Imaris was used, which were placed directly on the border of the selected vessel regions of interest. Correct placing of the measurement points was ensured by 3D inspection of the images.

Transient middle cerebral artery occlusion (tMCAO)

Focal cerebral ischaemia was induced by a transient MCA occlusion (tMCAO) as described[59]. Briefly, a silicon-coated thread was advanced through the carotid artery up to the origin of the MCA causing an MCA infarction. After an occlusion time of 60 min, the filament was removed allowing reperfusion of the MCA territory. The extent of oedema corrected brain infarction was quantitatively assessed 24 h after reperfusion on 2,3,5-triphenyltetrazolium chloride-stained consecutive brain sections. Neurological function

was analyzed calculating a neuroscore (score 0–10) based on the direct sum of the Grip test (score 0–5) and the inverted Bederson score (score 0–5).

PcomA scores

PcomA scores (posterior communicating artery) were determined in brains from mice that were perfused with PBS followed 3 ml black ink diluted in 4% PFA (1:5 v/v).

Mechanical injury of the abdominal aorta

To open the abdominal cavity of anaesthetised mice (8 to 20-weeks old), a longitudinal midline incision was performed, and the abdominal aorta was exposed. A Doppler ultrasonic flow probe (0.5PSB699, Transonic Systems, Maastricht, The Netherlands) was placed around the vessel and thrombus formation was induced by a single firm compression (20 s) with a forceps upstream of the flow probe. Blood flow was monitored over 30 min or until complete occlusion occurred (blood flow stopped for >5 min). The abdominal aorta was excised and embedded in Tissue Tek. Sections (5 μm) were fixed and stained according to Carstairs method to distinguish platelets and fibrin[60]. Images of Carstairs stained sections were acquired on a Leica DMI400B using the Leica Application Suite (LAS) software (version 2.6.0.R1).

$FeCl_3$-induced injury of mesenteric arterioles

4-weeks old mice were anaesthetised, and the mesentery was exteriorised. Arterioles (35–60 μm diameter) were visualised with a Zeiss Axiovert 200 inverted microscope (10x/0.25 air objective) equipped with a 100-W HBO mercury lamp and a CoolSNAP-EZ camera (Visitron, Munich, Germany) using Metamorph software (v6.2r6). Endothelial injury was induced by topical application of a 3 mm^2 filter paper saturated with ferric chloride ($FeCl_3$; 20%). Adhesion and aggregation of fluorescently labelled platelets (Dylight 488-conjugated anti-GPIX derivative) was monitored for 40 min or until complete occlusion occurred (blood flow stopped for >1 min).

Data analysis

The presented results are mean ± SD from three independent experiments per group and lines represent mean values, if not stated otherwise. Normal distribution was tested using the Shapiro-Wilk normality test. If passed, p-values were calculated using the two tailed unpaired t-test (2 groups), if the values were not normally distributed, differences between two groups were analysed using the Mann-Whitney two-tailed test. For more than two groups, one-way ANOVA (Kruskal-Wallis test) followed by Dunn’s test for multiple comparisons was performed using GraphPad Prism software (V7.03, 7.05.). Two tailed paired t-test (2 groups, normally distributed), Wilcoxon matched-pairs signed rank test (2 groups, not normally distributed) and Friedman test followed by Dunn’s test for multiple comparisons (more than 2 groups, not normally distributed) were used for paired comparisons. For statistical analysis of non-occluded vs. occluded vessels, Fisher’s exact t-test was used. P-values < 0.05 were considered statistically significant.

Extended Data

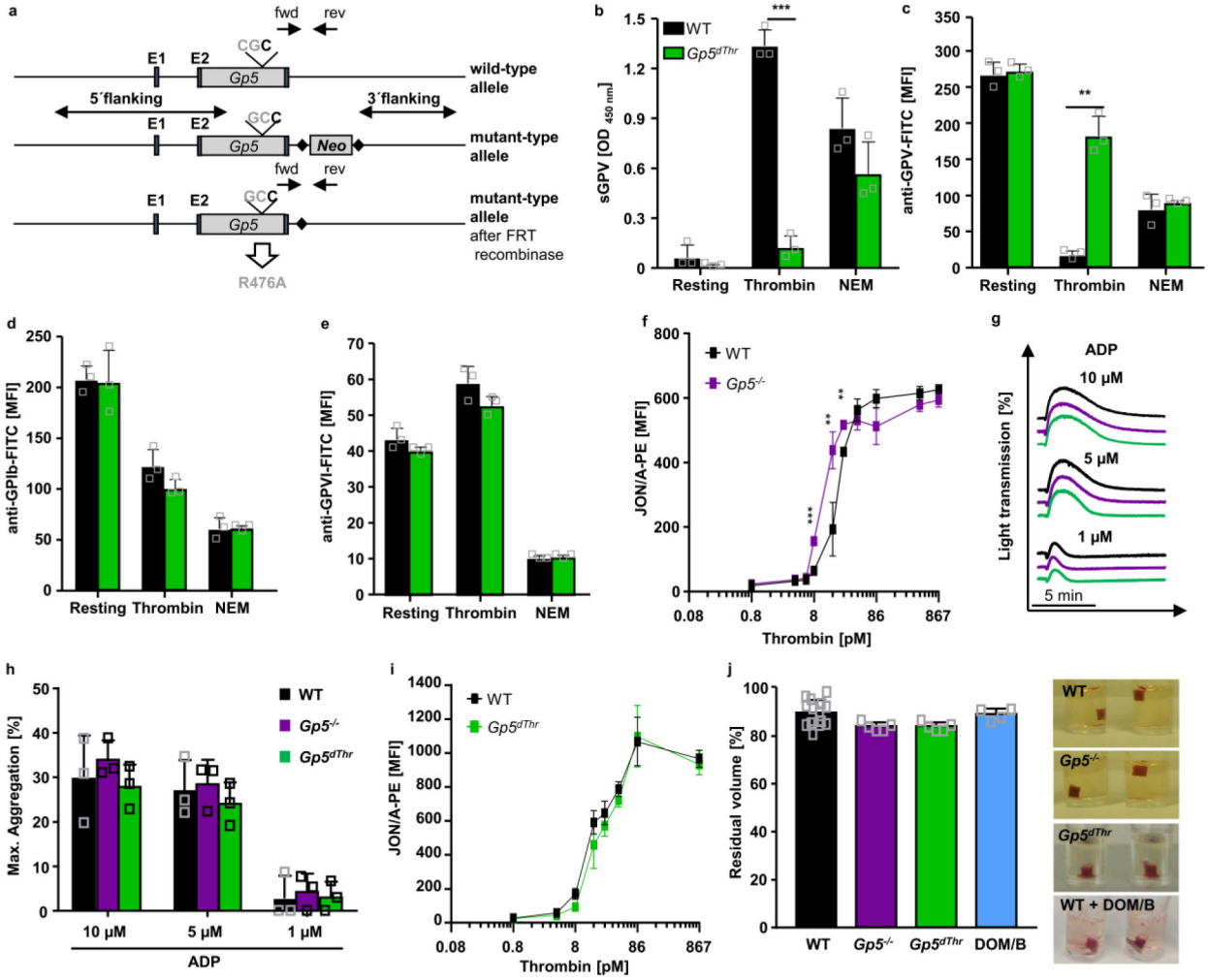

Extended Data Fig. 1. R476A point mutation renders GPV insensitive for thrombin-induced cleavage in *Gp5*^{dThr} mice but does not alter platelet reactivity towards thrombin.

(a) Simplified targeting strategy. *Gp5*^{dThr} mice were generated by introduction of the point mutation R476A in the thrombin cleavage site. **(b-e)** Washed platelets were left untreated or stimulated with 867 pM thrombin (in the presence of 40 µg/ml integrilin and 5 µM EGTA to prevent platelet aggregation) or 2 mM *N-ethylmaleimide* (NEM) to induce metalloproteinase-induced shedding of GPV. **(b)** After stimulation, sGPV levels in the platelet supernatant were measured using a mGPV ELISA. Mean ± SD. n=3 mice per group, 3 independent experiments, two-tailed unpaired t-test with Welch's correction, p=0.0001. **(c-e)** Stimulated platelets were incubated with saturating amounts of fluorophore-conjugated antibodies for 15 min at RT and the surface expression of GPV **(c)**, GPIb **(d)** and GPVI **(e)** was immediately analysed by flow cytometry. Mean ± SD. n=3 mice per group, 3 independent experiments, **(c)** two-tailed unpaired t-test with Welch's correction, p=0.0067. **(f)** Increased αIIbβ3 integrin activation measured by JON/A-PE staining of GPV-deficient platelets at threshold thrombin concentrations. Mean ± SD, n=4 mice, 5 independent experiments, two-tailed unpaired t-test with Welch's correction. 8.6 pM thrombin: p=0.0009,

17.35 pM thrombin: p=00039, 26 pM thrombin: p=0.0026 **(g, h)** Platelet-rich plasma (PRP) was stimulated with ADP and light transmission of PRP was recorded on a Apact four-channel aggregometer over 10 min. Representative curves **(g)** and maximum aggregation **(h)** for n=3 mice of 3 independent experiments expressed as mean ± SD. **(i)** Flow cytometry reveals unaltered reactivity of $Gp5^{dThr}$ platelets upon thrombin stimulation compared to WT controls. Mean ± SD, n=4 mice,5 independent experiments. **(j)** Clot formation in PRP was induced by the addition of thrombin and $CaCl_2$ and clot retraction was monitored over time. Residual volume of serum after clot retraction was measured. Mean ± SD. WT: n=14, $Gp5^{-/-}$: n=5, $Gp5^{dThr}$: n=5, WT + DOM/B: n=4 mice, 2 independent experiments. Representative images at 90 min after initiation of clot retraction. *$p < 0.05$; **$p < 0.01$; ***$p < 0.001$

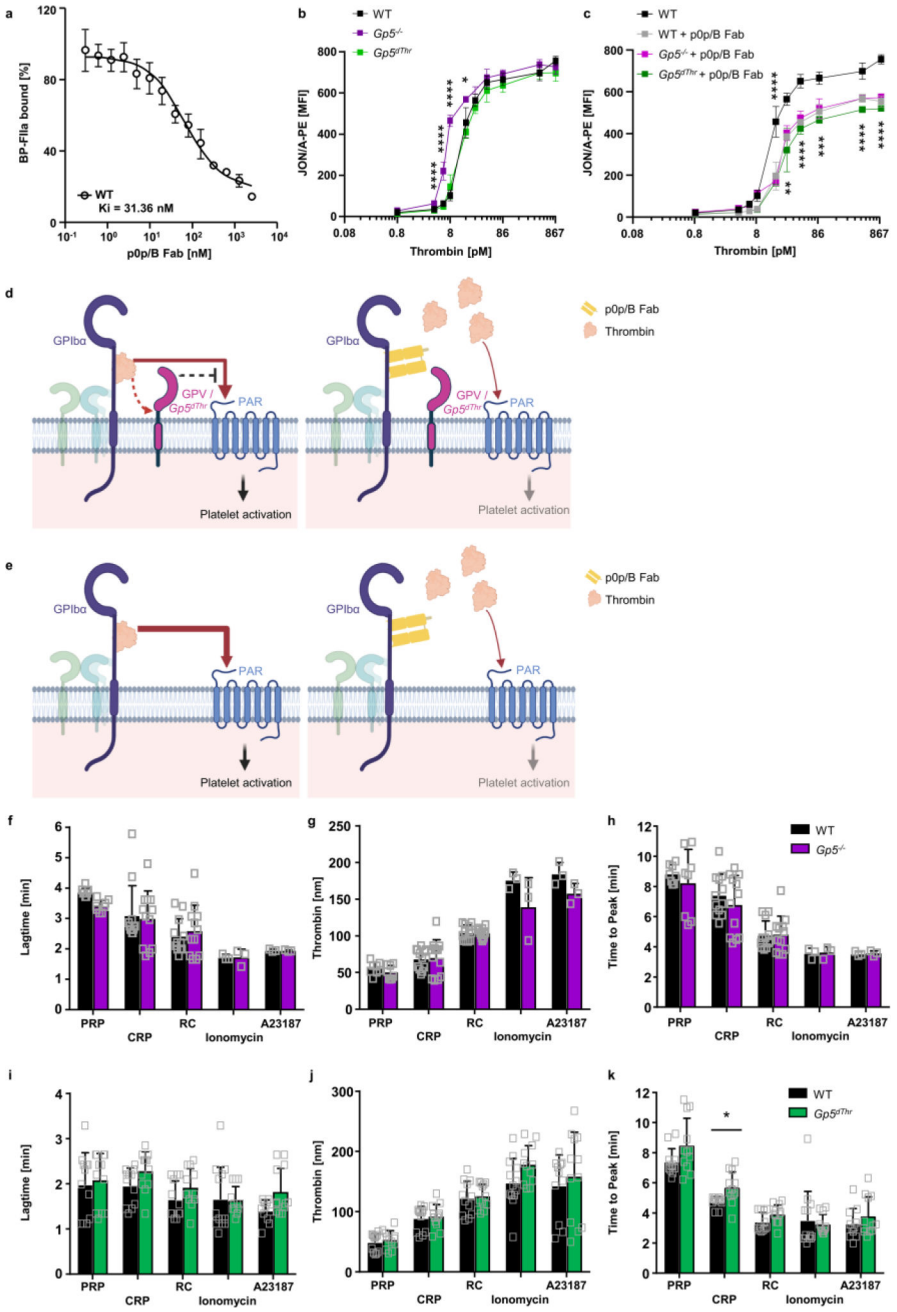

Extended Data Fig. 2. GPV regulates platelet responsiveness to thrombin by interference with GPIbα-dependent PAR signalling.

(a) Platelets were incubated with increasing concentrations of p0p/B Fab fragments and BP-FIIa binding was assessed by flow cytometry. n=4 mice, 2 independent experiments. **(b, c)** The thrombin-binding site on GPIbα was blocked by p0p/B Fab and αIIbβ3 integrin activation (JON/A-PE binding) of GPV-mutant and WT platelets measured by flow cytometry upon thrombin stimulation. **(b, c)** were measured in one experiment. Mean ± SD. n=4 mice per group, 4 independent experiments. One-way ANOVA followed by Tukey's multiple comparisons test. **(d)** Scheme of GPIb-thrombin and GPV-thrombin interactions. GPIX (green), GPIbβ (light blue), GPIbα and GPV (magenta) form a complex on the

platelet surface. Thrombin binds to GPIbα via a high affinity binding site, cleaves GPV and activates platelets via PARs. The anti-GPIbα Fab p0p/B blocks the thrombin binding site on GPIbα and thereby reduces thrombin-mediated platelet activation. Both, GPV and $Gp5^{dThr}$ act as an inhibitor of GPIb-mediated PAR activation. In the absence of GPV **(e)**, access of thrombin to PARs is facilitated leading to increased platelet activation. **(d, e)** created with BioRender. **(f-k)** TF-initiated thrombin generation was measured in platelet-rich plasma (PRP) upon platelet activation. Platelets were left unstimulated (PRP) or activated by incubation with collagen-related peptide (CRP) (20 μg/ml), rhodocytin (RC, 1 μg/ml), ionomycin (10 μM) or A23187 (10 μM) for 10 min at 37°C. Thrombin generation was triggered with tissue factor/$CaCl_2$. Lag time **(f, i)**, maximal thrombin concentration **(g, j)** and time to peak **(h, k)** were determined. Values are depicted as mean ± SD. **(f-h)** n=12 (CRP, RC), n=8 (PRP), n=3 (A23187, ionomycin). **(i-k)** n=12 (*Gp5*^{dThr}: all conditions, WT: PRP, CRP, RC); WT: n=13 (ionomycin), WT: n=11 (A23187) mice, at least 2 independent experiments. Two-tailed unpaired t-test with Welch's correction, p=0.0106. *$p < 0.05$; **$p < 0.01$; ***$p < 0.001$; ****$p < 0.0001$.

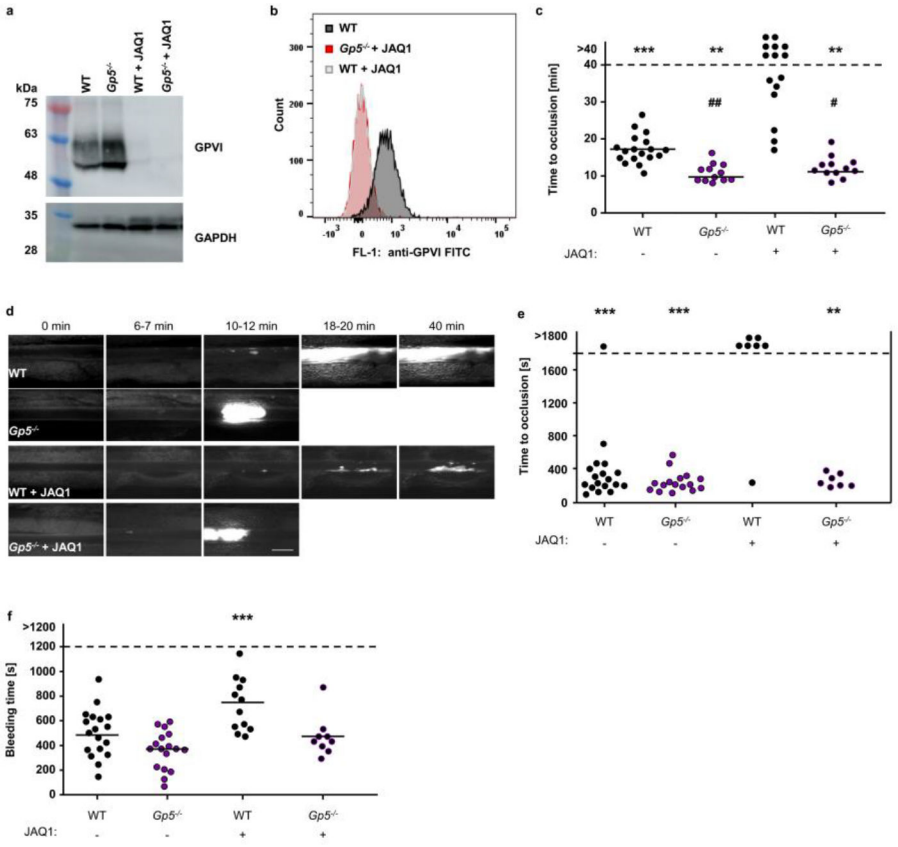

Extended Data Fig. 3. Absence of GPV restores thrombotic and haemostatic defects in the absence of GPVI.

GPVI was depleted from the platelet surface by injection of the anti-GPVI mAb JAQ1. Confirmation of GPVI depletion by Western blot analysis **(a)** and flow cytometry **(b)**; representative of 3 independent experiments. **(c)** Quantification and representative images (scale bar: 50 μm) **(d)** of thrombus formation upon $FeCl_3$-induced injury of mesenteric

arterioles. Thrombus formation in no more than two arterioles of each mouse were analysed; data points represent measurements of one arteriole. WT: 18 arterioles of 11 mice, *Gp5*$^{-/-}$:12 arterioles of 8 mice, WT + JAQ1: 15 arterioles of 8 mice, *Gp5*$^{-/-}$+ JAQ1: 12 arterioles of 7 mice. Two-tailed Fisher's exact test for open vs. occluded vessels, p=0.0005 (WT vs. WT +JAQ1), p=0.0031 (*Gp5*$^{-/-}$ vs. WT + JAQ1; *Gp5*$^{-/-}$ + JAQ1 vs. WT+JAQ1); one-way ANOVA followed by Tukey's test for multiple comparisons to compare occluded vessels, ## p= 0.0034 (WT vs. *Gp5*$^{-/-}$), # p=0.0401 (WT vs. *Gp5*$^{-/-}$ + JAQ1) compared to JAQ1-treated WT mice (p=0.0031). * compared to JAQ1-treated WT mice. **(e)** The abdominal aorta was mechanically injured by a single firm compression with a forceps and blood flow was monitored with a Doppler flowmeter. Time to cessation of blood flow is shown. Each symbol represents one mouse. Two-tailed Fisher's exact test for open vs. occluded vessels, one-way ANOVA followed by Dunn's test for multiple comparisons to compare occluded vessels. WT: n=18, *Gp5*$^{-/-}$: n=16, WT + JAQ1: n=7, *Gp5*$^{-/-}$+ JAQ1: n=7, ***WT +JAQ1 vs. WT and vs. *Gp5*$^{-/-}$: p<0.0001, ** WT +JAQ1 vs. *Gp5*$^{-/-}$+JAQ1: p=0.0047), ### compared to untreated WT mice (WT+JAQ1: p=0.0003). **(f)** Haemostatic function was assessed using a tail bleeding assay on filter paper. Each symbol represents one mouse. WT: n=18, *Gp5*$^{-/-}$: n=17, WT + JAQ1: n=12, *Gp5*$^{-/-}$+ JAQ1: n=9. one-way ANOVA followed by Dunn's test for multiple comparisons to compare occluded vessels, p=0.0001' *, $^{\#}$ $p < 0.05$; **, $^{\#\#}$ $p < 0.01$; ***, $^{\#\#\#}$ $p < 0.001$.

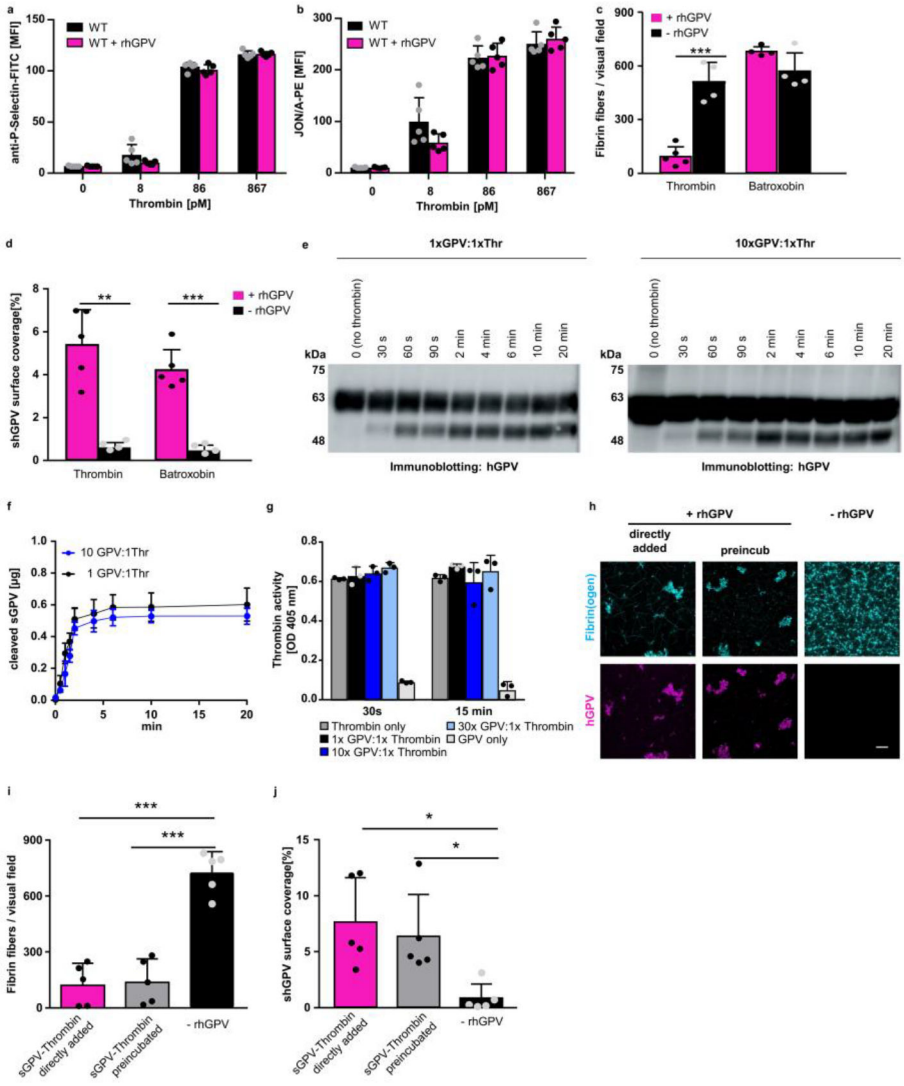

Extended Data Fig. 4. shGPV directly interacts with thrombin.

(a) P-selectin exposure at threshold thrombin concentrations in rhGPV-treated (20 µg/ml) and WT platelets. Mean ± SD of n=5 mice, 3 independent experiments. **(b)** Unaltered αIIbβ3 integrin activation (JON/A-PE binding) at threshold thrombin concentrations in the presence of rhGPV. Mean ± SD, n=5 mice, 3 independent experiments. Welch's test. Fibrin fibres **(c)** and hGPV staining **(d)** were quantified upon static fibrin polymerization induced by thrombin or batroxobin in the absence or presence of rhGPV. Mean ± SD, (c) -rhGPV: n=4, rhGPV: n=5 (Thrombin), n=4 (Batroxobin), two-tailed unpaired t-test with Welch's correction, p=0.0020, **(d)** -rhGPV: n=4, rhGPV: n=5 independent samples (mean of 2 ROI per sample), two-tailed unpaired t-test wit Welch's correction, p=0.0029 (thrombin), p=0.0006 (batroxobin). **(e-g)** rhGPV and thrombin were incubated at equimolar ratio (1:1) or with an excess of rhGPV (10:1 ratio) and thrombin-mediated cleavage of rhGPV was assessed over time by immunoblotting. **(f)** Quantification of thrombin-cleaved sGPV over time. Mean ± SD, n=5 independent western blot experiments. **(g)** rhGPV and thrombin were incubated at equimolar ratio (1:1) or with an excess of rhGPV (10:1, 30:1 ratio) and the

activity of thrombin was determined using a chromogenic thrombin substrate. Mean ± SD, n=3 independent samples, representative of 4 experiments. **(h)** Maximum projection of static fibrin polymerization induced by thrombin in the absence or presence of rhGPV (30:1 ratio). Thrombin and rhGPV were either directly added or preincubated for 10 min prior induction of polymerization. Fluorophore labelled fibrin(ogen): cyan, staining for hGPV: magenta. Scale bar: 20 μm. Quantification of fibrin fibres **(i)** and hGPV staining **(j)**. Mean ± SD. n=5 biologic samples (mean of 2 ROI per sample), **(i)** one-way ANOVA followed by Tukey's multiple comparison test, p>0.0001, **(j)** Kruskal-Wallis test followed by Dunn's multiple comparisons test, p=0.0175 (directly vs. no rhGPV), p=0.0327 (preincubated vs. no rhGPV). *, $p < 0.05$; **$p < 0.01$; ***$p < 0.001$.

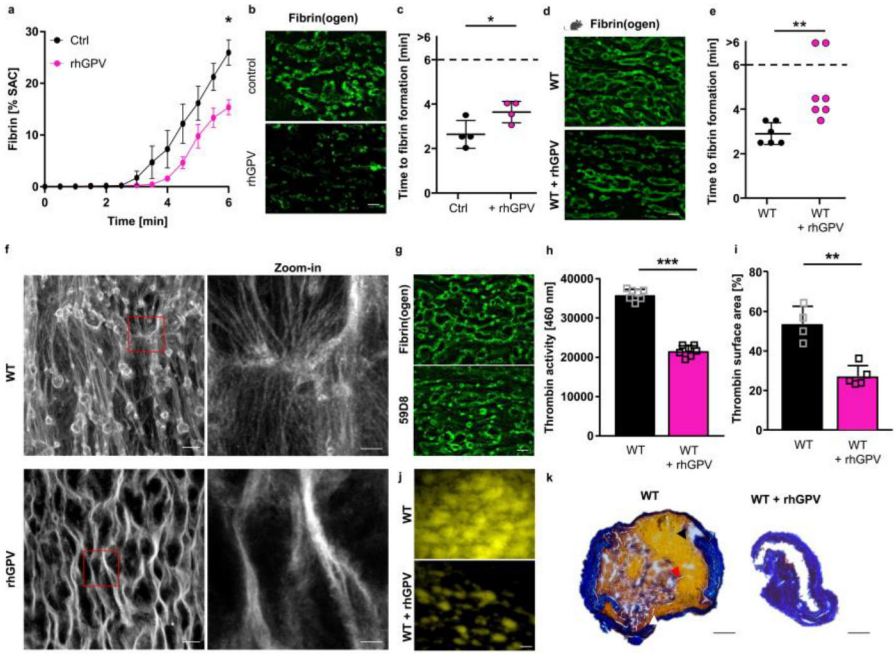

Extended Data Fig. 5. rhGPV delays and reduces fibrin formation.

Recalcified whole blood was incubated *in vitro* with 20 μg/ml rhGPV prior to perfusion over collagen/TF spots. Quantification of fibrin generation during blood flow in human **(a-c)** and mouse blood **(d, e)**. **(a)** Mean ± SEM; n=4 donors, 3 independent experiments, two-tailed paired t-test, p=0.0133. Ctrl: human donor. **(b, d)** Representative images displaying decreased fibrin formation after rhGPV-treatment. Scale bar: 20 μm. **(c)** Time to fibrin formation in rhGPV-treated human blood. Ctrl: Human control. Mean ± SD, n=4 donors, 3 independent experiments, two-tailed paired t-test, p=0.0163. **(e)** Time to fibrin formation in rhGPV-treated WT blood. Mean ± SD, WT: n=6, WT+rhGPV: n=7, 3 independent experiments, two-tailed Mann-Whitney test, p=0.0023. **(f)** Analysis of fibrin fibrils by laser scanning confocal microscopy. Fibrin fibres were visualised using a Leica SP8 confocal microscope, 63x oil, Hyvolution mode, z-step size: 0.1 μm, 15 μm z-size. Images were deconvolved using Huygens Software. Maximum projection. Scale bar: 20 μm. Zoom-in: 5 μm. Representative of n=5 mice. **(g)** Fibrin formation using Fibrin(ogen)A488 or the anti-Fibrin antibody 59D8. Representative images, scale bar: 20 μm. **(h)** Thrombin activity was determined in the outflow of the flow chamber using a fluorogenic thrombin substrate

and measured immediately after sample collection. Mean ± SD; n=7 mice, 3 independent experiments, two-tailed unpaired t-test with Welch's correction, p<0.0001. **(i)** Thrombin activity in flow chambers was determined using the fluorogenic thrombin substrate Z-GGR-AMC. **(j)** Representative images of **(i)**. Mean ± SD; WT: n=4, WT + rhGPV: n=5 mice, 2 independent experiments, two-tailed unpaired t-test with Welch's correction, p=0.0039. Scale bar: 20 µm. **(k)** Carstairs staining of the abdominal aorta after mechanical injury-induced thrombus formation in a WT and rhGPV-treated mouse (red blood cells: yellow (indicated with black arrowhead), fibrin: bright red (red arrowhead), platelets: navy blue (white arrowhead), collagen: blue). Scale bar: 100 µm. rhGPV: 20 µg/ml. SAC: surface area coverage. *$p < 0.05$; **$p < 0.01$; ***$p < 0.001$.

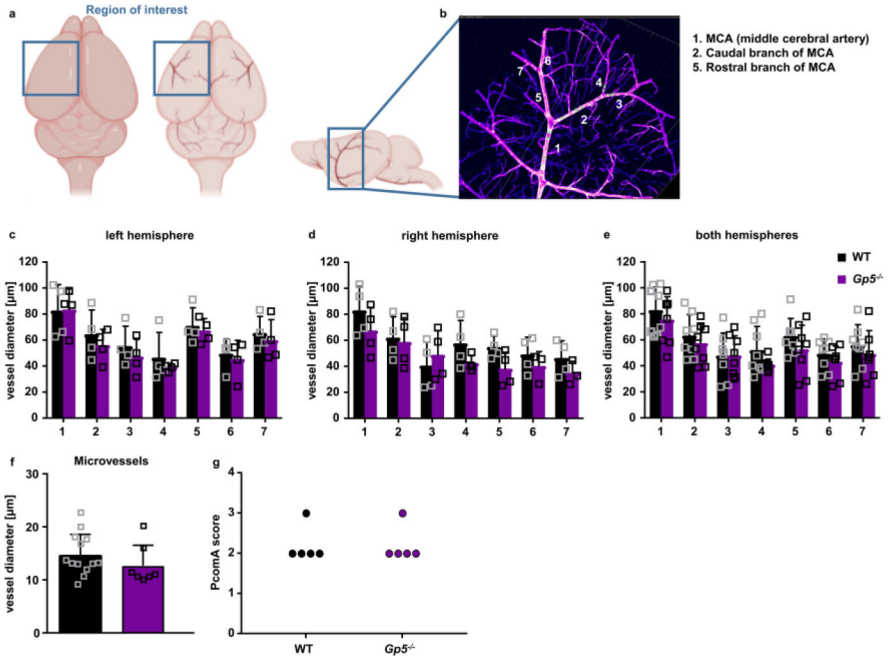

Extended Data Fig. 6. Unaltered MCA vessel diameter in *Gp5*$^{-/-}$ mice.

Optically transparent brain samples of *Gp5*$^{-/-}$ and WT mice were imaged using light sheet fluorescence microscopy (LSFM). **(a)** Due to its conserved branching and its easy recognition, we focused on the region around the middle cerebral artery (MCA) to allow better comparability between the samples. **(b)** We analysed the vessel diameter of the MCA (1) and 2 subsequent branches of the caudal (2) and rostral (5) branch of the MCA using Imaris Software. **(c-e)** Vessels in the left, right hemisphere and the combination of both hemispheres did not show any difference between GPV-deficient and WT mice. Mean ± SD. n=4 mice. **(f)** Vessel diameters of microvessels in the brain were comparable between *Gp5*$^{-/-}$ and WT mice. Mean ± SD. WT: n=13 vessels of 4 mice, *Gp5*$^{-/-}$: n=7 vessels of 4 mice. Two-tailed unpaired t-test with Welch's correction. **(g)** PcomA scores (posterior communicating artery) were determined in brains from mice that were perfused with PBS followed 3 ml black ink diluted in 4% PFA (1:5 v/v) and comparable between *Gp5*$^{-/-}$ and WT mice. n=5. Mann-Whitney test. (a, b) created with BioRender.

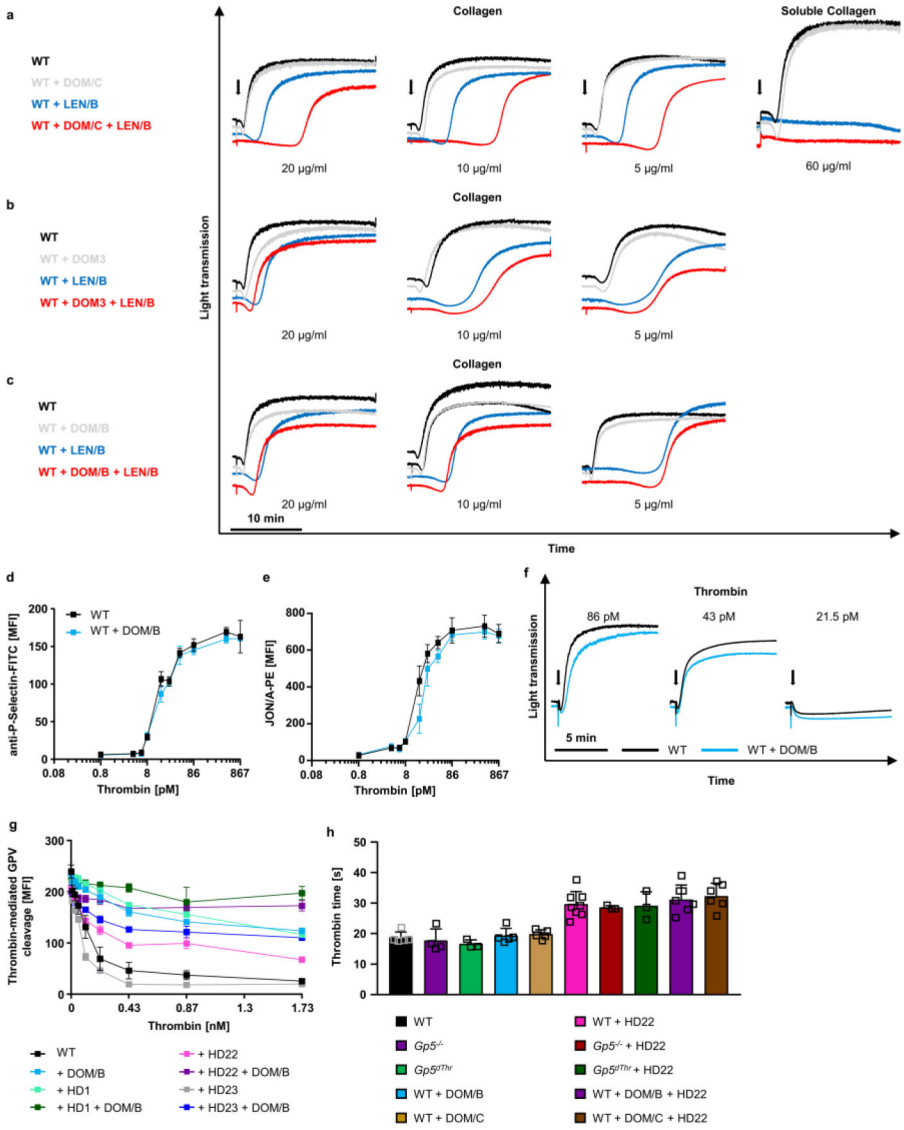

Extended Data Fig. 7. DOM/B does not alter platelet responses upon stimulation with collagen or thrombin *in vitro*, despite interfering with thrombin-mediated cleavage of GPV.

(a-c) Washed platelets were incubated *in vitro* with 10 µg/ml of the indicated antibodies for 5 min and stimulated with Horm or soluble collagen. Light transmission was recorded on an Apact four-channel aggregometer over 20 min. Representative aggregation curves of n=3, 2 independent experiments. LEN/B: anti-α2 integrin antibody[51]. **(d, e)** Flow cytometry reveals unaltered reactivity of DOM/B-treated WT platelets upon thrombin stimulation compared to WT controls. Mean ± SD. n=3 mice, 4 independent experiments, two-tailed unpaired t-test with Welch's correction. **(f)** Aggregation upon thrombin-stimulation is not affected in the presence of DOM/B. Light transmission was recorded on an Apact four-channel aggregometer over 10 min. Representative curves of n=3, 3 individual experiments. **(g)** Thrombin exosites I and II were blocked by the aptamers HD1 and HD22, respectively. Platelets were incubated with the indicated antibody (10 µg/ml) prior to thrombin stimulation. Thrombin-mediated cleavage of GPV was assessed by flow cytometry.

Mean ± SD. n=3 mice, 3 independent experiments. **(h)** Thrombin clotting time was assessed using a ball coagulometer in GPV mutant or anti-mGPV mAb treated PRP in the presence or absence of HD22. Antibody concentration: 10 µg/ml; aptamer concentration: 1.5 µM f.c., thrombin: 17 nM. Mean ± SD. WT, WT+DOM/B, WT+DOM/C: n=5, *Gp5*$^{-/-}$: n=4, *Gp5*^{dThr}, *Gp5*$^{-/-}$+HD22, *Gp5*^{dThr}+HD22: n=3, WT+DOM/B+HD22, WT+DOM/C+HD22: n=6, WT+HD22: n=8. One-way ANOVA followed by Dunn's test for multiple comparisons.

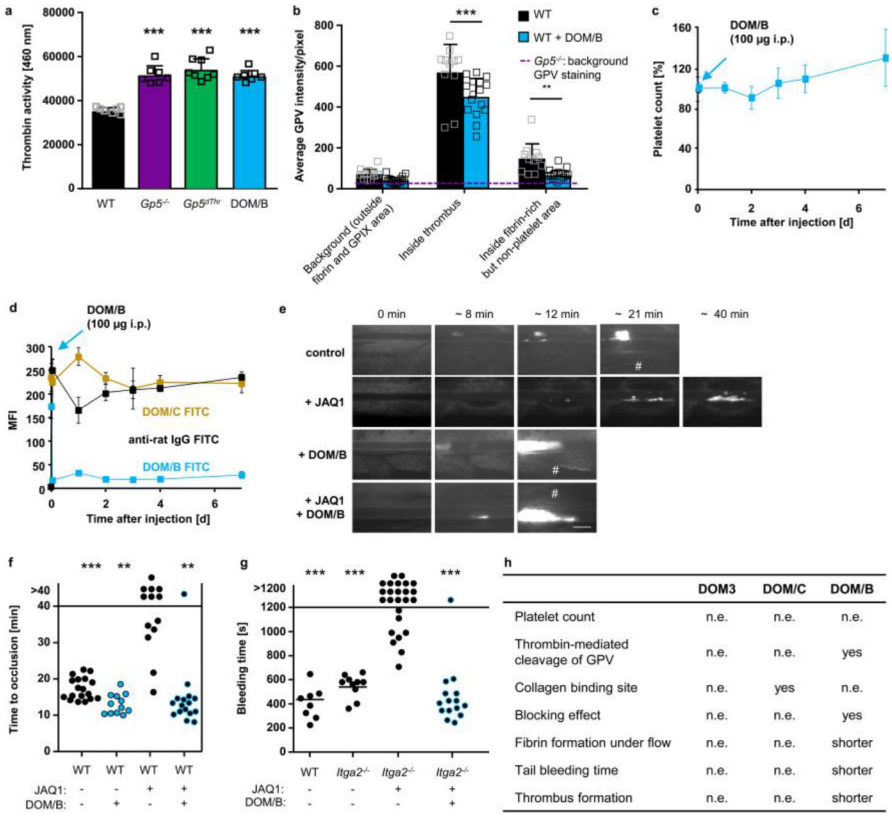

	DOM3	DOM/C	DOM/B
Platelet count	n.e.	n.e.	n.e.
Thrombin-mediated cleavage of GPV	n.e.	n.e.	yes
Collagen binding site	n.e.	yes	n.e.
Blocking effect	n.e.	n.e.	yes
Fibrin formation under flow	n.e.	n.e.	shorter
Tail bleeding time	n.e.	n.e.	shorter
Thrombus formation	n.e.	n.e.	shorter

Extended Data Fig. 8. DOM/B restores haemostasis and thrombus formation in the absence of GPVI, thereby reproducing the *Gp5*$^{-/-}$ phenotype.

(a) Recalcified blood was perfused over collagen/TF spots. Thrombin activity was determined in the outflow using a fluorogenic thrombin substrate and measured immediately. Mean ± SD. WT, *Gp5*$^{-/-}$, WT+DOM/B: n=7, *Gp5*^{dThr}: n=8, one-way ANOVA followed by Tukey's multiple comparisons test, p<0.0001 for all groups compared to WT. **(b)** Recalcified blood was perfused over collagen/TF spots. Samples were stained for platelets (anti-GPIX), fibrin(ogen) and GPV, fixed and analysed with a Zeiss Airyscan microscope. Quantification of GPV intensities inside fibrin-rich, non-platelet area. Background GPV intensity in *Gp5*$^{-/-}$ images is displayed as dashed line (n=4). Mean ± SD. Two-way ANOVA followed by Tukey's multiple comparisons test, p<0.0001 (inside thrombus), p=0.0089 (inside fibrin), WT. n=11, WT+DOM/B: n=16. **(c, d)** WT mice were injected with DOM/B (100 µg i.p.) and platelet count was assessed for 7 days **(c)**. Platelet count at d0 was set to 100%. Mean ± SD. n=5 mice, 2 independent experiments. **(d)** GPV platelet surface expression was assessed by flow cytometry for up to 7 days after DOM/B injection. Mean ± SD. n=5 mice, 2 independent experiments. Receptor opsonisation

was measured using an anti-rat IgG FITC antibody. **(e-g)** GPVI was depleted from the platelet surface by injection of the anti-GPVI mAb JAQ1. Representative images **(e)** and quantification **(f)** of thrombus formation upon $FeCl_3$-induced injury of mesenteric arterioles in WT mice after JAQ1 and DOM/B treatment. Thrombus formation in no more than two arterioles of each mouse was analysed; data points represent measurements of one arteriole. WT: n=18 arterioles of 10 mice, WT+DOM/B: n=12 arterioles of 6 mice, WT+JAQ1: n=13 arterioles of 7 mice, WT+DOM/B+JAQ1: n=16 arterioles of 8 mice, two-tailed Fisher's exact test to compare occluded vs. non-occluded vessels was used. p=0.0007 (vs. WT), p=0.0052 (vs. WT+DOM/B), p=0.0011 (vs. WT+JAQ1+DOM/B), # indicates vessel occlusion. Scale bar: 50 μm. **(g)** Mice lacking both collagen receptors GPVI and α2 were treated with DOM/B and haemostatic function was assessed using a tail bleeding assay on filter paper. Each symbol represents one mouse. WT: n=8, *Itga2*$^{-/-}$: n=10, *Itga2*$^{-/-}$ + JAQ1: n=25, *Itga2*$^{-/-}$ + JAQ1 + DOM/B: n=16, two-tailed Fisher's exact test for open vs. occluded vessels. p=0.0009 (vs. WT), p=0.0003 (vs. *Itga2*$^{-/-}$), p=0.0001 (vs. *Itga2*$^{-/-}$+JAQ1 +DOM/B), **(h)** Summary of the effects of the different anti-mGPV antibodies. n.e.: no effect. *$p < 0.05$; **$p < 0.01$; ***$p < 0.001$.

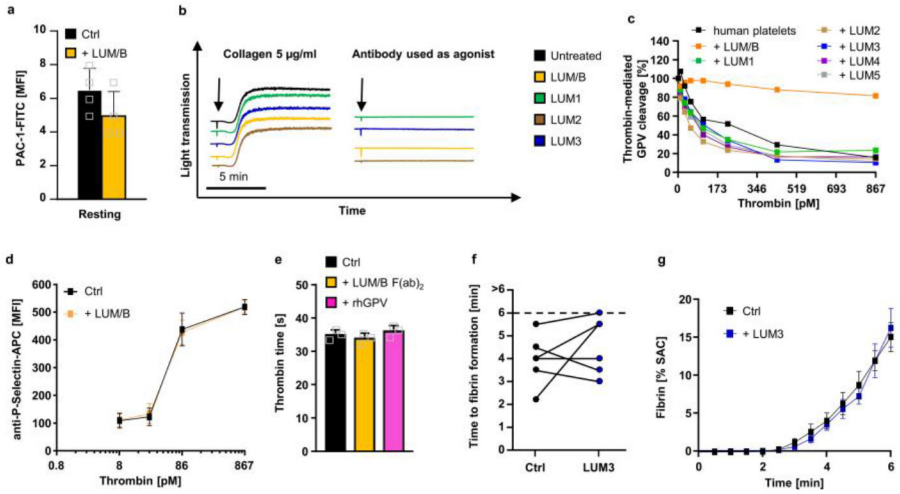

Extended Data Fig. 9. LUM/B has no effect on thrombin-mediated platelet activation.

(a) Human platelets were incubated with 10 μg/ml LUM/B prior to flow cytometric analysis of PAC1-binding. Mean ± SD, n=4 donors. **(b)** Human platelets were incubated with the indicated anti-hGPV mAbs light transmission was recorded on a Apact four-channel aggregometer over 10 min. Representative curves for n=3. **(c)** Human platelets were incubated with the indicated antibody (10 μg/ml) prior to thrombin stimulation. Thrombin-mediated cleavage of GPV was assessed by flow cytometry. Mean ± SD, n=2 donors, 3 independent experiments. **(d)** Flow cytometry reveals unaltered reactivity of LUM/B-treated platelets upon thrombin stimulation compared to controls. **(e)** Neither blockade of hGPV by LUM/B $F(ab)_2$ nor rhGPV (290 nM) affect thrombin time. **(a, c, d, e)** Values are displayed as mean ± SD. **(d)** n=4 donors, 3 independent experiments, two-tailed unpaired t-test with Welch's correction. **(e)** n=3 donors, one-way ANOVA. **(f, g)** Recalcified whole blood was incubated *in vitro* with 10 μg/ml anti-hGPV antibody LUM3 prior to perfusion over collagen/TF spots. Quantification time to fibrin formation **(f)** and fibrin surface coverage

(g) during blood flow of LUM3-treated (n=8 donors) and control samples (n=10 donors). *(f)* n=6 donors Values are depicted as mean ± SEM **(g)**. SAC: Surface area coverage. Ctrl: Human donor.

Extended Data Table 1.

Analysis of platelet count, size, and surface expression of glycoproteins in Gp5dThr mice.

Mean platelet count and size were determined using a Sysmex cell counter. Surface expression of platelet glycoproteins was determined by flow cytometry. Diluted whole blood was stained with FITC-labelled antibodies at saturating amounts for 15 min at RT. Platelets were analysed immediately on a FACSCalibur. Results are expressed as mean fluorescence intensity (MFI) ± SD. n=4–6, two-tailed unpaired t-test with Welch's correction, *p < 0.05.

	WT	*Gp5^{dThr}*	P-value	Sig.
Count	85.8 ±25.0	102.8 ±20.4	0.2460	n.s.
MPV	5.4 ±0.2	5.5 ± 0.2	0.4678	n.s.
WBC [10/µl]	76.7 ±21.6	76.0 ±15.2	0.95355473	n.s.
RBC [1E4/µl]	89.0 ± 25	93.2 ±3,1	0,70015665	n.s.
HGB [g/µl]	1.4 ±0.3	1.5 ± 0.1	0.43026063	n.s.
HCT [%]	4.8 ± 1.3	5.1 ±0.2	0.52205469	n.s.
GPIb [MFI]	341.3 ±20.3	354.3 ± 5.3	0.29312226	n.s.
GPV [MFI]	318.5 ± 11.9	289 ±32.6	0.1203	n.s.
GPIX [MFI]	308.75 ± 8.66	317.75 ±4.79	0.13244492	n.s.
GPVI [MFI]	33.25 ±0.96	34 ±1.41	0.41799623	n.s.
$\alpha_{IIb}\beta 3$ [MFI]	338.75 ± 27.68	353 ± 14.53	0.4216117	n.s.
β3 [MFI]	157.8 ±43.6	153.2 ±5.7	0.8260	n.s.
α5 [MFI]	18 ±0.01	18 ±0.03 2	1	n.s.
α2 [MFI]	38.75 ± 0.957	39.25 ±3.59	0.80343776	n.s.
CD9 [MFI]	669.75 ±45.15	746 + 2.83	0.04258772	*
CLEC-2 [MFI]	90.75 ± 6.24	82.5 ± 15.26	0.37396966	n.s.
CD84 [MFI]	25 ± 1.63	25.5 ±0.58	0.59667799	n.s.

Supplementary Material

Refer to Web version on PubMed Central for supplementary material.

Acknowledgments:

We thank F. Lanza (Strasbourg, France) for providing *Gp5$^{-/-}$* mice, J. Pinnecker (Julius-Maximilians-Universität Würzburg, Würzburg, Germany) for assistance in LSFM image acquisition, S. Hartmann and J. Goldmann for excellent technical assistance (both: University Hospital Würzburg, Institute of Experimental Biomedicine, Würzburg, Germany) and M. Spindler for excellent graphical assistance (University Hospital Würzburg, Institute of Experimental Biomedicine, Würzburg, Germany).

Funding:

German Research Foundation Ni556/14-1 (BN)

German Research Foundation (SFB 1525, project number: 453989101)

German Research Foundation (TR240, project number: 374031971)

National Institutes of Health grant HL082808 (RL) and UM1 HL120877 (WR)

German Research Foundation INST 93/1022-1

European Union (Thrombo-Inflame, EFRE–Europäischer Fonds für regionale Entwicklung, Bavaria)

Rudolf Virchow Centre for Integrative and Translational Bioimaging

Data availability:

All data supporting the analyses presented in this study are provided in the manuscript and associated files.

References

1. Swieringa F, Spronk HMH, Heemskerk JWM & van der Meijden PEJ Integrating platelet and coagulation activation in fibrin clot formation. Res Pract Thromb Haemost 2, 450–460, doi:10.1002/rth2.12107 (2018). [PubMed: 30046749]
2. Furie B & Furie BC The molecular basis of blood coagulation. Cell 53, 505–518, doi:10.1016/0092-8674(88)90567-3 (1988). [PubMed: 3286010]
3. Tomaiuolo M, Brass LF & Stalker TJ Regulation of platelet activation and coagulation and its role in vascular injury and arterial thrombosis. Interv Cardiol Clin 6, 1–12, doi:10.1016/j.iccl.2016.08.001 (2017). [PubMed: 27886814]
4. Kahn ML et al. A dual thrombin receptor system for platelet activation. Nature 394, 690–694, doi:10.1038/29325 (1998). [PubMed: 9716134]
5. Stalker TJ et al. Hierarchical organization in the hemostatic response and its relationship to the platelet-signaling network. Blood 121, 1875–1885, doi:10.1182/blood-2012-09-457739 (2013). [PubMed: 23303817]
6. Versteeg HH, Heemskerk JW, Levi M & Reitsma PH New fundamentals in hemostasis. Physiol. Rev. 93, 327–358, doi:10.1152/physrev.00016.2011 (2013). [PubMed: 23303912]
7. Sang Y, Roest M, de Laat B, de Groot PG & Huskens D Interplay between platelets and coagulation. Blood Rev. 46, 100733, doi:10.1016/j.blre.2020.100733 (2021). [PubMed: 32682574]
8. Silva LM et al. Fibrin is a critical regulator of neutrophil effector function at the oral mucosal barrier. Science 374, eabl5450, doi:10.1126/science.abl5450 (2021). [PubMed: 34941394]
9. Ryu JK et al. Fibrin-targeting immunotherapy protects against neuroinflammation and neurodegeneration. Nat. Immunol. 19, 1212–1223, doi:10.1038/s41590-018-0232-x (2018). [PubMed: 30323343]
10. Mosnier LO, Zlokovic BV & Griffin JH The cytoprotective protein C pathway. Blood 109, 3161–3172, doi:10.1182/blood-2006-09-003004 (2006). [PubMed: 17110453]
11. Ruggeri ZM et al. Unravelling the mechanism and significance of thrombin binding to platelet glycoprotein Ib. Thromb. Haemost. 104, 894–902, doi:10.1160/TH10-09-0578 (2010). [PubMed: 20941453]
12. Kahn ML et al. Glycoprotein V-deficient platelets have undiminished thrombin responsiveness and Do not exhibit a Bernard-Soulier phenotype. Blood 94, 4112–4121 (1999). [PubMed: 10590056]
13. Li R & Emsley J The organizing principle of the platelet glycoprotein Ib-IX-V complex. J. Thromb. Haemost. 11, 605–614, doi:10.1111/jth.12144 (2013). [PubMed: 23336709]
14. Mo X, Liu L, Lopez JA & Li R Transmembrane domains are critical to the interaction between platelet glycoprotein V and glycoprotein Ib-IX complex. J. Thromb. Haemost. 10, 1875–1886, doi:10.1111/j.1538-7836.2012.04841.x (2012). [PubMed: 22759073]
15. Moog S et al. Platelet glycoprotein V binds to collagen and participates in platelet adhesion and aggregation. Blood 98, 1038–1046 (2001). [PubMed: 11493449]

16. Nieswandt B & Watson SP Platelet-collagen interaction: is GPVI the central receptor? Blood 102, 449–461, doi:10.1182/blood-2002-12-3882 (2003). [PubMed: 12649139]
17. Clemetson KJ A short history of platelet glycoprotein Ib complex. Thromb. Haemost. 98, 63–68 (2007). [PubMed: 17597992]
18. Katsutani S et al. Cloning and characterization of the gene encoding the murine glycoprotein V: the conserved thrombin-cleavable protein on platelet surface. Thromb. Res. 92, 43–51, doi:10.1016/s0049-3848(98)00111-x (1998). [PubMed: 9783673]
19. Ravanat C et al. Gene cloning of rat and mouse platelet glycoprotein V: identification of megakaryocyte-specific promoters and demonstration of functional thrombin cleavage. Blood 89, 3253–3262 (1997). [PubMed: 9129030]
20. Ni H Increased thrombogenesis and embolus formation in mice lacking glycoprotein V. Blood 98, 368–373, doi:10.1182/blood.V98.2.368 (2001). [PubMed: 11435305]
21. Rabie T, Strehl A, Ludwig A & Nieswandt B Evidence for a role of ADAM17 (TACE) in the regulation of platelet glycoprotein V. J. Biol. Chem. 280, 14462–14468, doi:10.1074/jbc.M500041200 (2005). [PubMed: 15691827]
22. Ramakrishnan V et al. Increased thrombin responsiveness in platelets from mice lacking glycoprotein V. Proc. Natl. Acad. Sci. U. S. A. 96, 13336–13341 (1999). [PubMed: 10557321]
23. Nonne C, Hechler B, Cazenave JP, Gachet C & Lanza F Reassessment of in vivo thrombus formation in glycoprotein V deficient mice backcrossed on a C57Bl/6 strain. J. Thromb. Haemost. 6, 210–212, doi:10.1111/j.1538-7836.2007.02825.x (2008). [PubMed: 17988230]
24. McGowan EB, Ding A & Detwiler TC Correlation of thrombin-induced glycoprotein V hydrolysis and platelet activation. J. Biol. Chem. 258, 11243–11248 (1983). [PubMed: 6309838]
25. Estevez B et al. Signaling-mediated cooperativity between glycoprotein Ib-IX and protease-activated receptors in thrombin-induced platelet activation. Blood 127, 626–636, doi:10.1182/blood-2015-04-638387 (2016). [PubMed: 26585954]
26. Celikel R et al. Modulation of α-thrombin function by distinct interactions with platelet glycoprotein Ibα. Science 301, 218, doi:10.1126/science.1084183 (2003). [PubMed: 12855810]
27. Dumas JJ, Kumar R, Seehra J, Somers WS & Mosyak L Crystal structure of the GpIbalpha-thrombin complex essential for platelet aggregation. Science 301, 222–226, doi:10.1126/science.1083917 (2003). [PubMed: 12855811]
28. Massberg S et al. A crucial role of glycoprotein VI for platelet recruitment to the injured arterial wall in vivo. J. Exp. Med. 197, 41–49 (2003). [PubMed: 12515812]
29. Stegner D et al. Foudroyant cerebral venous (sinus) thrombosis triggered through CLEC-2 and GPIIb/IIIa dependent platelet activation. Nature Cardiovascular Research 1, 132–141, doi:10.1038/s44161-021-00017-1 (2022).
30. Bender M et al. Combined in vivo depletion of glycoprotein VI and C-type lectin-like receptor 2 severely compromises hemostasis and abrogates arterial thrombosis in mice. Arterioscler. Thromb. Vasc. Biol. 33, 926–934, doi:10.1161/ATVBAHA.112.300672 (2013). [PubMed: 23448972]
31. Nieswandt B et al. Long-term antithrombotic protection by in vivo depletion of platelet glycoprotein VI in mice. J. Exp. Med. 193, 459–469, doi:10.1084/jem.193.4.459 (2001). [PubMed: 11181698]
32. Mangin P et al. Thrombin overcomes the thrombosis defect associated with platelet GPVI/FcRγ deficiency. Blood 107, 4346–4353, doi:10.1182/blood-2005-10-4244 (2006). [PubMed: 16391010]
33. Mangin PH et al. Immobilized fibrinogen activates human platelets through glycoprotein VI. Haematologica 103, 898–907, doi:10.3324/haematol.2017.182972 (2018). [PubMed: 29472360]
34. de Witt SM et al. Identification of platelet function defects by multi-parameter assessment of thrombus formation. Nature communications 5, 4257, doi:10.1038/ncomms5257 (2014).
35. Nagy M et al. Comparative analysis of microfluidics thrombus formation in multiple genetically modified mice: link to thrombosis and hemostasis. Front Cardiovasc Med 6, 99, doi:10.3389/fcvm.2019.00099 (2019). [PubMed: 31417909]
36. Fredenburgh JC, Stafford AR, Leslie BA & Weitz JI Bivalent binding to gammaA/gamma'-fibrin engages both exosites of thrombin and protects it from inhibition by the antithrombin-heparin complex. J. Biol. Chem. 283, 2470–2477, doi:10.1074/jbc.M707710200 (2008). [PubMed: 18055456]

37. Stoll G & Nieswandt B Thrombo-inflammation in acute ischaemic stroke - implications for treatment. Nat. Rev. Neurol. 15, 473–481, doi:10.1038/s41582-019-0221-1 (2019). [PubMed: 31263257]
38. Petrera NS et al. Long range communication between exosites 1 and 2 modulates thrombin function. J. Biol. Chem. 284, 25620–25629, doi:10.1074/jbc.M109.000042 (2009). [PubMed: 19589779]
39. Bock LC, Griffin LC, Latham JA, Vermaas EH & Toole JJ Selection of single-stranded DNA molecules that bind and inhibit human thrombin. Nature 355, 564–566, doi:10.1038/355564a0 (1992). [PubMed: 1741036]
40. Tasset DM, Kubik MF & Steiner W Oligonucleotide inhibitors of human thrombin that bind distinct epitopes. J. Mol. Biol. 272, 688–698, doi:10.1006/jmbi.1997.1275 (1997). [PubMed: 9368651]
41. Grüner S et al. Anti–glycoprotein VI treatment severely compromises hemostasis in mice with reduced α2β1 levels or concomitant aspirin therapy. Circulation 110, 2946–2951, doi:10.1161/01.CIR.0000146341.63677.3C (2004). [PubMed: 15505105]
42. Pleines I et al. Megakaryocyte-specific RhoA deficiency causes macrothrombocytopenia and defective platelet activation in hemostasis and thrombosis. Blood 119, 1054–1063, doi:10.1182/blood-2011-08-372193 (2012). [PubMed: 22045984]
43. Deppermann C et al. Gray platelet syndrome and defective thrombo-inflammation in Nbeal2-deficient mice. J. Clin. Invest. 123, 3331–3342, doi:10.1172/JCI69210 (2013). [PubMed: 23863626]
44. Bakchoul T & Marini I Drug-associated thrombocytopenia. Hematology Am. Soc. Hematol. Educ. Program 2018, 576–583, doi:10.1182/asheducation-2018.1.576 (2018). [PubMed: 30504360]
45. Aster RH & Bougie DW Drug-induced immune thrombocytopenia. N. Engl. J. Med. 357, 580–587, doi:10.1056/NEJMra066469 (2007). [PubMed: 17687133]
46. Morowski M et al. Only severe thrombocytopenia results in bleeding and defective thrombus formation in mice. Blood 121, 4938–4947, doi:10.1182/blood-2012-10-461459 (2013). [PubMed: 23584880]
47. Sekhon UDS et al. Platelet-mimicking procoagulant nanoparticles augment hemostasis in animal models of bleeding. Sci. Transl. Med. 14, eabb8975, doi:10.1126/scitranslmed.abb8975 (2022). [PubMed: 35080915]
48. Mast AE & Ruf W Regulation of coagulation by tissue factor pathway inhibitor: Implications for hemophilia therapy. J. Thromb. Haemost. 20, 1290–1300, doi:10.1111/jth.15697 (2022). [PubMed: 35279938]
49. Holtkotter O et al. Integrin alpha 2-deficient mice develop normally, are fertile, but display partially defective platelet interaction with collagen. J. Biol. Chem. 277, 10789–10794, doi:10.1074/jbc.M112307200 (2002). [PubMed: 11788609]
50. Jackson B et al. RhoA is dispensable for skin development, but crucial for contraction and directed migration of keratinocytes. Mol. Biol. Cell 22, 593–605, doi:10.1091/mbc.E09-10-0859 (2011). [PubMed: 21209320]
51. Knight CG et al. Collagen-platelet interaction: Gly-Pro-Hyp is uniquely specific for platelet Gp VI and mediates platelet activation by collagen. Cardiovasc. Res. 41, 450–457, doi:Doi 10.1016/S0008-6363(98)00306-X (1999). [PubMed: 10341844]
52. Hemker HC & Beguin S Thrombin generation in plasma: its assessment via the endogenous thrombin potential. Thromb. Haemost. 74, 134–138 (1995). [PubMed: 8578446]
53. Hemker HC et al. Calibrated automated thrombin generation measurement in clotting plasma. Pathophysiol. Haemost. Thromb. 33, 4–15, doi:10.1159/000071636 (2003). [PubMed: 12853707]
54. Brouns SLN et al. Platelet-primed interactions of coagulation and anticoagulation pathways in flow-dependent thrombus formation. Sci. Rep. 10, 11910, doi:10.1038/s41598-020-68438-9 (2020). [PubMed: 32680988]
55. van der Walt S et al. scikit-image: image processing in Python. PeerJ 2, e453, doi:10.7717/peerj.453 (2014). [PubMed: 25024921]
56. Schindelin J et al. Fiji: an open-source platform for biological-image analysis. Nat. Methods 9, 676–682, doi:10.1038/nmeth.2019 (2012). [PubMed: 22743772]

57. Göb V et al. Infarct growth precedes cerebral thrombosis following experimental stroke in mice. Sci. Rep. 11, 22887, doi:10.1038/s41598-021-02360-6 (2021). [PubMed: 34819574]

58. Amich J et al. Three-dimensional light sheet fluorescence microscopy of lungs to dissect local host immune-aspergillus fumigatus interactions. mBio 11, doi:10.1128/mBio.02752-19 (2020).

59. Kleinschnitz C et al. Targeting platelets in acute experimental stroke: impact of glycoprotein Ib, VI, and IIb/IIIa blockade on infarct size, functional outcome, and intracranial bleeding. Circulation 115, 2323–2330, doi:10.1161/CIRCULATIONAHA.107.691279 (2007). [PubMed: 17438148]

60. Carstairs KC The identification of platelets and platelet antigens in histological sections. J. Pathol. Bacteriol. 90, 225–231, doi:10.1002/path.1700900124 (1965). [PubMed: 5320852]

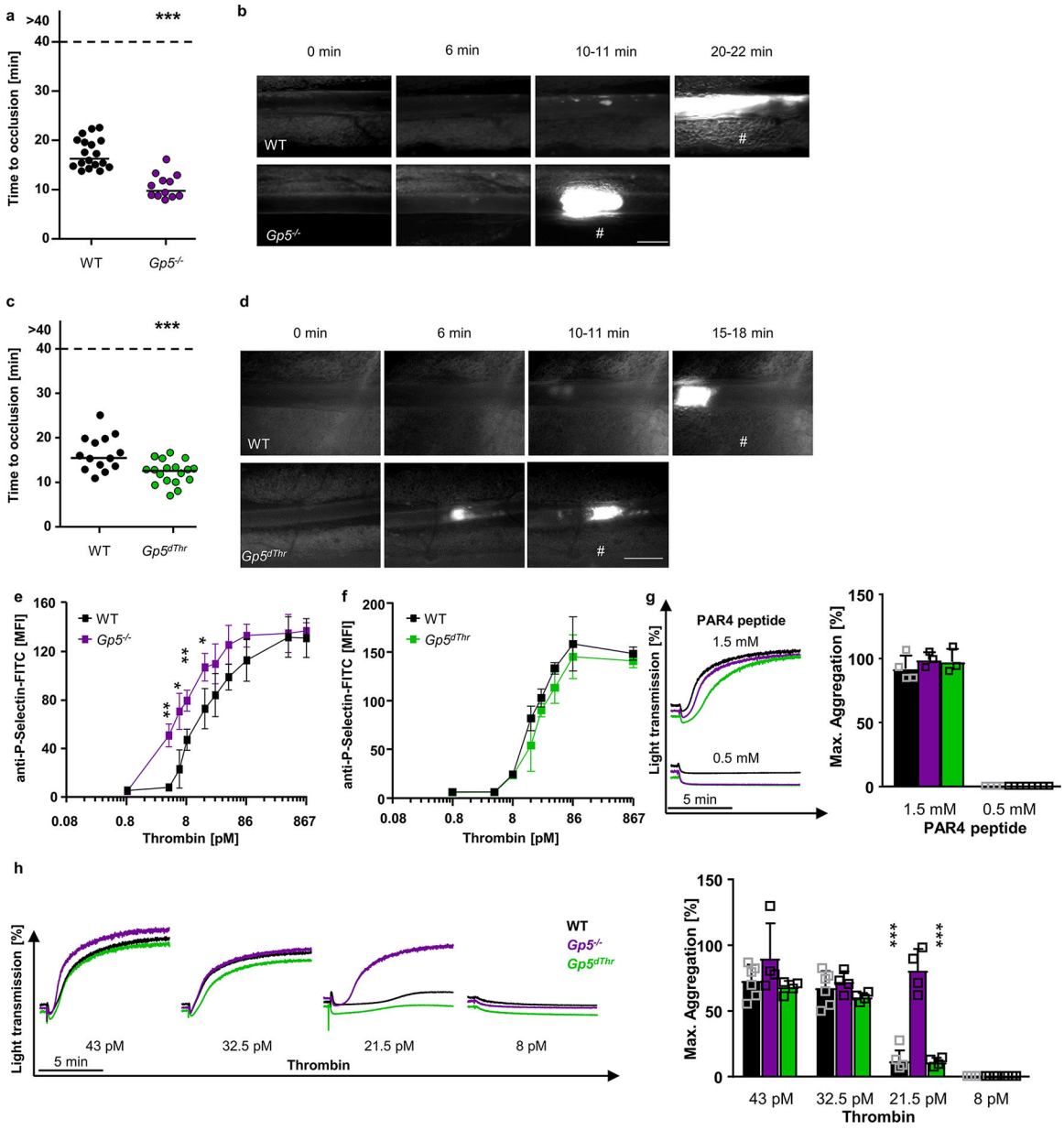

Fig. 1. Platelet thrombin hyperresponsiveness and accelerated thrombus formation in GPV mutant mice.

(a) Quantification and **(b)** representative images of thrombus formation upon $FeCl_3$-induced injury of mesenteric arterioles in *Gp5*$^{-/-}$ or WT mice. Thrombus formation in no more than two arterioles of each mouse were analysed; data points represent measurements of one arteriole. WT: n=18 arterioles of 11 mice, *Gp5*$^{-/-}$ n=12 arterioles of 7 mice, two-tailed unpaired t-test, p<0.0001. scale bar: 50 µm. **(c)** Quantification of thrombus formation and **(d)** representative images upon $FeCl_3$-induced injury of mesenteric arterioles in *Gp5*^{dThr} or WT mice. At most two arterioles of each mouse were analysed. Each dot represents one arteriole. #: indicates occlusive thrombus formation. WT: n=14 arterioles of 10 mice, *Gp5*^{dThr} n=18 arterioles of 9 mice, two-tailed unpaired t-test, p=0.0010. scale bar: 50 µm. **(e)** Increased P-selectin exposure of GPV-deficient platelets at threshold thrombin

concentrations. Mean±SD, n=4 mice per group, 5 independent experiments, two-tailed unpaired t-test with Welch's correction. 4.3 pM thrombin: p=0.0025, 6.45 pM thrombin: p=0.0286, 8.6 pM thrombin: p=0.0020, 17.2 pM thrombin: p=0.0179 **(f)** Flow cytometry reveals unaltered reactivity of *Gp5*^{dThr} platelets upon thrombin stimulation compared to WT controls. Mean±SD, n=4 mice per group, 5 independent experiments. **(g, h)**Washed platelets were stimulated with the indicated agonists and light transmission of washed platelets upon stimulation with the indicated PAR4 peptide (g) or thrombin (h) concentrations was recorded on a Apact four-channel aggregometer over 10 min. Representative curves for (g) n=4, (h) n=4 (*Gp5*$^{-/-}$; *Gp5*^{dThr}); n=4–6 for WT of 3 independent experiments. Maximum aggregation expressed as mean ± SD. WT vs. *Gp5*$^{-/-}$ and *Gp5*$^{-/-}$ vs. *Gp5*^{dThr}: p<0.0001. One-way ANOVA followed by Tukey's multiple comparisons test. Strain matched controls were used. *p < 0.05; **p < 0.01; ***p < 0.001.

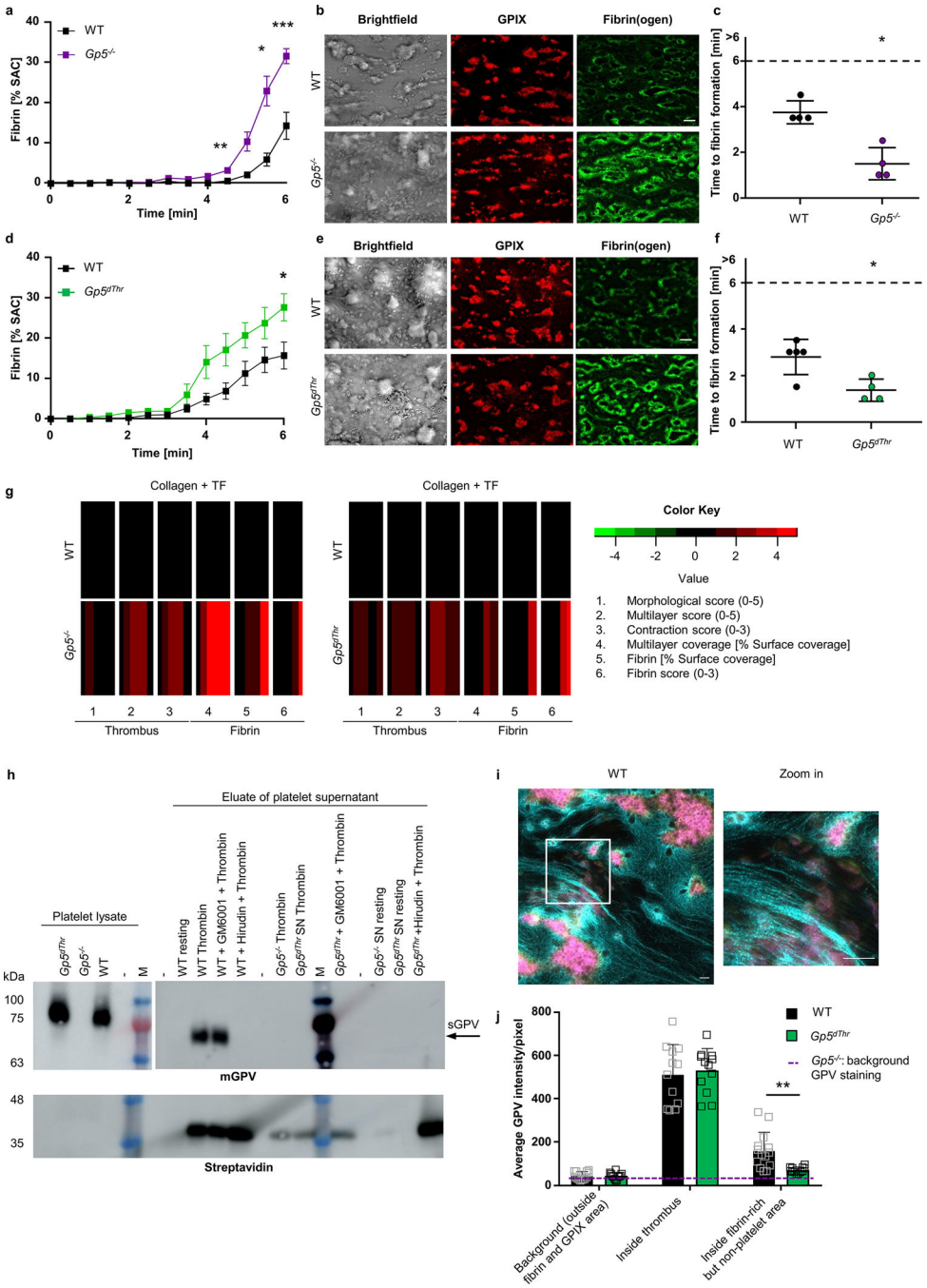

Fig. 2. GPV alters fibrin formation and localises to fibrin fibres outside the thrombus after thrombin cleavage.

(a) Time-dependent fibrin generation of *Gp5*$^{-/-}$ and WT mice was quantified. Mean ± SEM, WT: n=9, *Gp5*$^{-/-}$: n= 8, 3 independent experiments. Two-tailed unpaired t-test with Welch's correction. 4.5 min: p=0.0072, 5.5 min: p=0.0296, 6 min: p=0.0006. **(b)** Representative images of thrombus formation (anti-GPIX-AF647: red) and fibrin formation (fibrin(ogen)-AF488: green) on collagen/TF spots after 6 min. Scale bar: 20 µm. **(c)** Quantification of time to fibrin formation. One dot represents one animal. Mean ± SD, n=4, Two-tailed

Mann-Whitney test. p=0.0286. **(d-f)** Fibrin formation on collagen/TF microspots of *Gp5*^{dThr} and WT mice. Quantification of fibrin formation **(d),** time to fibrin formation **(f)** and representative images **(e)**. Scale bar: 20 μm. Staining see (b). (d) mean ± SEM, WT: n=6, *Gp5*^{dThr}: n=8, Two-tailed unpaired t-test with Welch's correction. 6 min: p=0.0287. (f) Mean ± SD, WT: n=5, *Gp5*^{dThr}: n=4, Two-tailed Mann-Whitney test. p=0.0317. SAC: surface area coverage. **(g)** Subtraction heatmap of parameters of thrombus (increased multilayer and contraction score) and fibrin formation in mutant mice compared to WT controls. Colours represent unchanged (black), decreased (green) or increased (red) parameters. **(h)** Pulldown of sGPV from WT platelets using streptavidin beads after stimulation with biotinylated thrombin in the presence/absence of GM6001 (matrix metalloproteinase inhibitor). No pulldown of sGPV from *Gp5*^{dThr} platelets nor in the presence of hirudin, which prevents GPV cleavage by thrombin. Eluates were analysed by Western blotting using GPV-specific antibodies and streptavidin-HRP. Representative result of 5 independent experiments. M: marker, mGPV: murine GPV, arrow indicates pulldown of sGPV. **(i, j)** Recalcified blood was perfused over collagen/TF microspots. Samples were stained for platelets (anti-GPIX: yellow), fibrin(ogen) (cyan) and GPV (magenta), and analysed with a Zeiss Airyscan microscope. **(i)** Representative WT image and Zoom-in. Scale bar: 4 μm. **(j)** Quantification of GPV intensities inside fibrin-rich, but non-platelet area. Background GPV intensity in *Gp5*$^{-/-}$ images is displayed as dashed line. Two-way ANOVA followed by Tukey's multiple comparisons test, n=14 (WT), n=12 (*Gp5*^{dThr}), n=4 (*Gp5*$^{-/-}$) ROI representing n=4 mice. Mean ± SD, p=0.0086. For detailed analysis see Supplementary Fig. 1. *p < 0.05; **p < 0.01; ***p < 0.001.

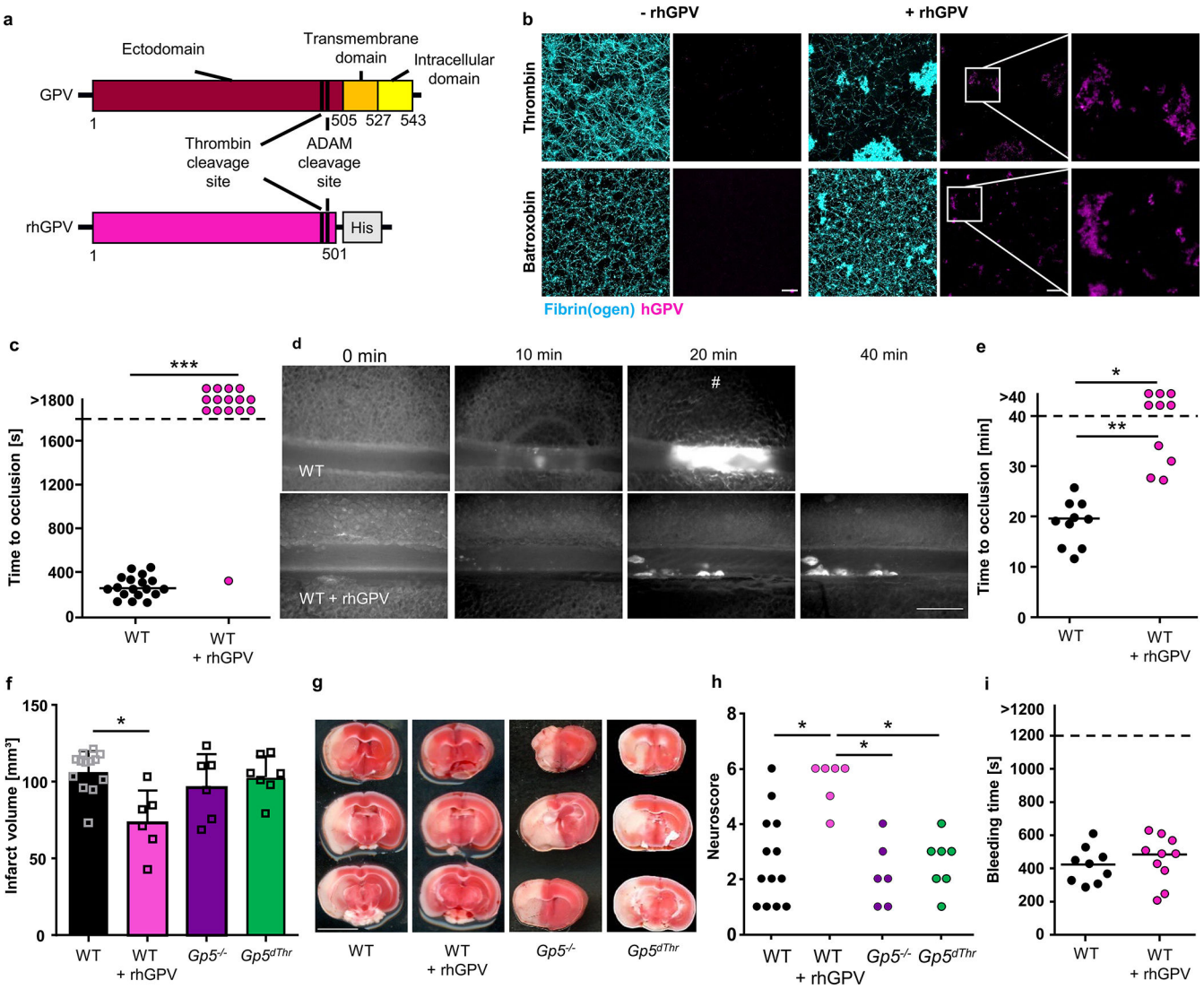

Fig. 3. rhGPV reduces fibrin formation and thereby protects from occlusive thrombosis and ischaemic stroke.

(a) Simplified scheme of full-length and recombinant ectodomain of human GPV. rhGPV contains the thrombin and ADAM cleavage sites and a C-terminal His-tag. **(b)** Maximum projection of static fibrin polymerization induced by thrombin (upper panel) or batroxobin (lower panel) in the absence or presence of rhGPV (see Extended Data Fig. 4c, d for quantification). Fluorophore labelled fibrin(ogen): cyan, staining for hGPV: magenta. Scale bar: 20 µm. **(c)** Quantification of thrombus formation after mechanical injury of the abdominal aorta. WT: n=18, WT+rhGPV: n=15, Two-tailed Fisher's exact test. $p<0.0001$. **(d)** Representative images (#: indicates occlusive thrombus formation; scale bar: 50 µm) and **(e)** quantification of thrombus formation upon $FeCl_3$-induced injury of mesenteric arterioles of rhGPV-treated and WT mice. WT: n=10 arterioles of 5 mice, WT+rhGPV: n=10 arterioles of 6 mice, Two-tailed Fisher's exact test foropen vs. occluded vessels: WT vs. rhGPV: p=0.0108, Two-tailed Mann Whitney test for comparison of occluded vessels: p=0.002. **(f)** Quantification of infarct volumes in tMCAO model of ischaemic stroke. Mean ± SD, WT:

n=13, WT+rhGPV: n=6, *Gp5*$^{-/-}$: n=6, *Gp5*^{dThr}: n=7, two-tailed Kruskal-Wallis test with Dunn's post-test, p=0.0298.. Of note, rhGPV-treatment neither triggered large intracranial haemorrhages, nor elevated mortality (WT: 2/15; WT+rhGPV: 1/7; *Gp5*$^{-/-}$: 0/6, *Gp5*^{dThr}: 1/8). **(g)** Three consecutive TTC-stained brain sections of one representative mouse. white: infarct; red: viable tissue. Scale bar: 0.5 cm. **(h)** Neuroscore displaying behavioural outcome after tMCAO. WT vs. WT + rhGPV: p=0.0135, WT + rhGPV vs. *Gp5*$^{-/-}$: p=0.0116, WT + rhGPV vs. *Gp5*^{dThr}: p=0.0440, one-way ANOVA followed by Dunn's test for multiple comparisons. **(i)** Unaltered tail bleeding time after rhGPV-treatment. WT: n=9, WT+rhGPV: n=10. rhGPV: 20 μg/mouse injected prior to surgery. *p < 0.05; **p < 0.01; ***p < 0.001.

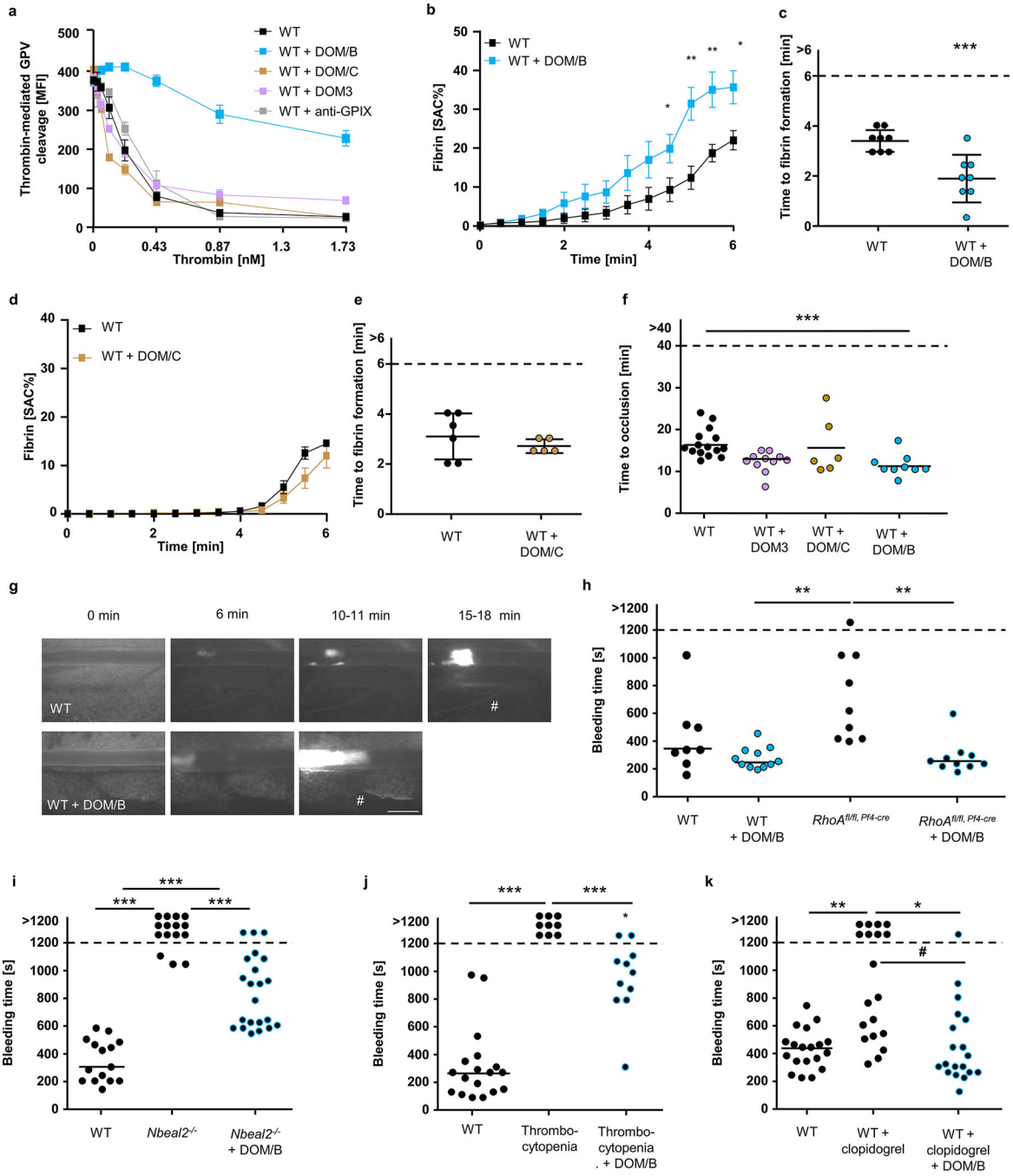

Fig. 4. The anti-mGPV antibody DOM/B interferes with thrombin-mediated cleavage of GPV and reproduces the *Gp5*$^{-/-}$ phenotype.

(a) Thrombin-mediated cleavage of GPV was assessed by flow cytometry. Mean ± SD, n=3, 4 independent experiments. **(b-e)** Recalcified whole blood was incubated *in vitro* with 10 μg/ml anti-mGPV antibody prior to perfusion over collagen/TF spots. Quantification of fibrin generation during blood flow **(b, d)** and time to fibrin formation **(c, e)**. (b) Mean ± SEM, n=8, 3 independent experiments, two-tailed unpaired t-test with Welch's correction. 4.5 min: p=0.0430; 5 min: p=0.0029; 5.5 min: p= 0.0092; 6 min: p=0.0186. (c) Mean ±

SD, n=8, 4 independent experiments, two-tailed unpaired t-test, p=0.0010. (d) Mean ± SEM, n=3, 3 independent experiments. (**e**) Mean ± SD, 3 independent experiments, WT: n=6, WT+DOM/C: n=5. SAC: Surface area coverage. **(f)** Quantification and **(g)** representative images of thrombus formation upon $FeCl_3$-induced injury of mesenteric arterioles. WT (= WT + control IgG): n=15 arterioles of 8 mice, WT+DOM3: n=11 arterioles of 6 mice, WT+DOM/C: n=6 arterioles of 4 mice, WT+DOM/B: n=9 arterioles of 6 mice. DOM/B vs. WT: p=0.0008. #: indicates occlusive thrombus formation. Scale bar: 50 μm. **(h-k)** Tail bleeding time assays. (h) WT (with control IgG): n=8, WT+DOM/B: n=11, *RhoA*$^{fl/fl,\ Pf4\text{-}cre}$: n=9, *RhoA*$^{fl/fl,\ Pf4\text{-}cre}$+DOM/B: n=10. *RhoA*$^{fl,\ fl\ Pf4\text{-}cre}$+ DOM/B vs. *RhoA*$^{fl,fl\ Pf4\text{-}cre}$: p=0064; DOM/B vs. *RhoA*$^{fl,\ fl\ Pf4\text{-}cre}$: p=0.002. (i) WT (with control IgG): n=15, *Nbeal2*$^{-/-}$: n=15, *Nbeal2*$^{-/-}$+DOM/B: n=22. Open vs. occluded vessels: WT vs. *Nbeal2*$^{-/-}$: p< 0.0001, *Nbeal2*$^{-/-}$ + DOM/B vs. *Nbeal2*$^{-/-}$: p<0.0001, comparison of occluded vessels: *Nbeal2*$^{-/-}$ + DOM/B vs. WT: p<0.0001; WT vs. *Nbeal2*$^{-/-}$: p=0.0006. **(j)** WT mice were injected with platelet depletion antibody to induce thrombocytopenia (5–10% of normal counts). WT (with control IgG): n=18, Thrombocytopenia: n=9, Thrombocytopenia +DOM/B: n=11, Open vs. occluded vessels: WT vs. thrombocytopenic mice: p< 0.0001, thrombocytopenic mice +DOM/B vs. thrombocytopenic mice: p=0.0003, Comparison of occluded vessels: thrombocytopenic mice +DOM/B vs. WT: p=0.0251. (k) n=19 (all groups). Open vs. occluded vessels: WT vs. WT + clopidogrel: p=0.0031, WT + DOM/B + clopidogrel vs. WT + clopidogrel: p=0.0188, Comparison of occluded vessels: WT + DOM/B + clopidogrel vs. WT + clopidogrel: $^{\#}$p=0.0383. (f, h-k) Two tailed Kruskal-Wallis Test followed by Dunn's multiple comparison test to compare occluded vessels. Two-tailed Fisher's exact test was used to compare occluded vs. non-occluded vessels. *, $^{\#}$ p < 0.05; **p < 0.01; ***p < 0.001.

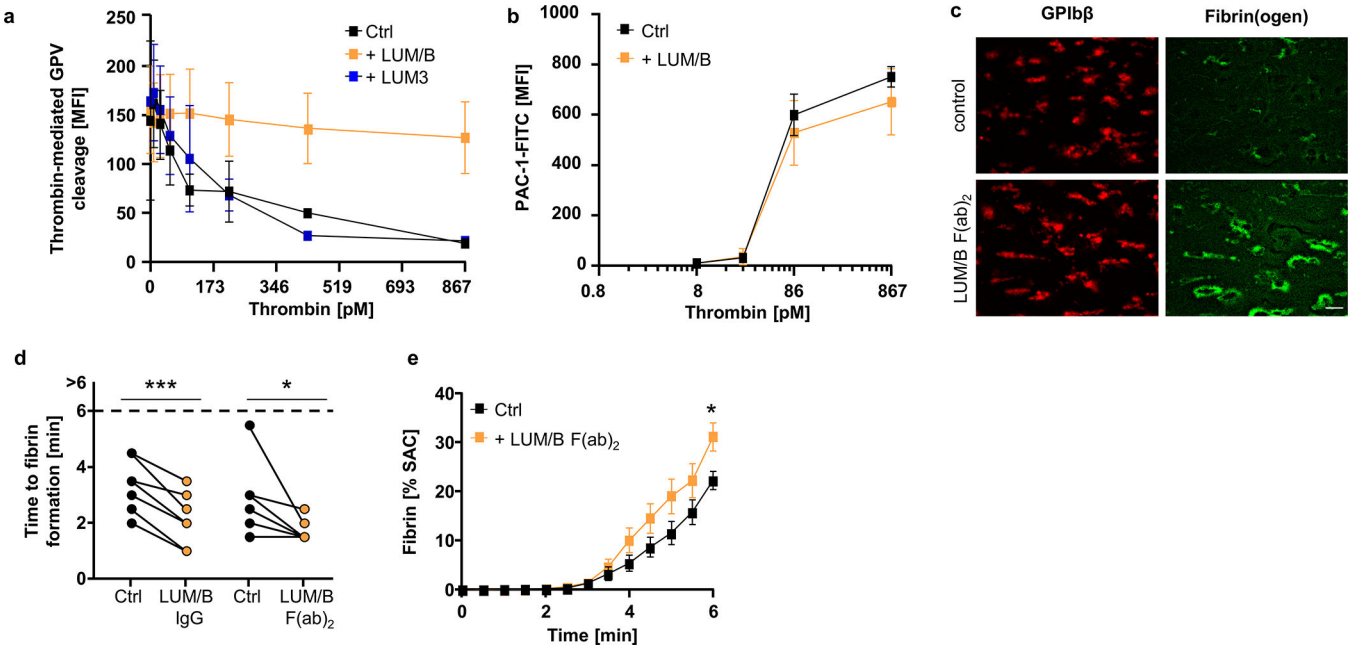

Fig. 5. The anti-hGPV mAb LUM/B interferes with thrombin cleavage and accelerates fibrin formation.

(a) Human platelets were incubated with the indicated antibody or control IgG (10 μg/ml) prior to thrombin stimulation. Thrombin-mediated cleavage of GPV was assessed by flow cytometry. Mean ± SD, n=4 donors, 3 independent experiments. **(b)** Flow cytometry reveals unaltered reactivity of LUM/B-treated platelets (10 μg/ml) upon thrombin stimulation compared to human controls. Mean ± SD, n=4 donors, 3 independent experiments. **(c-e)** Recalcified whole blood was incubated with LUM/B IgG or LUM/B $F(ab)_2$ prior to perfusion over collagen/TF spots. **(c)** Representative images of thrombus (GPIbβ) and fibrin formation. Scale bar: 20 μm. Quantification of time to fibrin formation **(d)** and fibrin generation during blood flow **(e)** after LUM/B-treatment. SAC: surface area coverage. (d) Ctrl vs. LUM/B IgG: n=7, two-tailed paired t-test; Ctrl vs. LUM/B $F(ab)_2$: n=7, Two-tailed Wilcoxon matched pairs signed rank test, Ctrl vs. 1B1 IgG: p=0.006; Ctrl vs. 1B1 $F(ab)_2$: p=0.0313. (e) mean ± SEM. n=10 donors, 3 independent experiments. Two-tailed unpaired t-test, 6 min: p=0.0159. Ctrl: Human donor. *p < 0.05; **p < 0.01; ***p < 0.001.

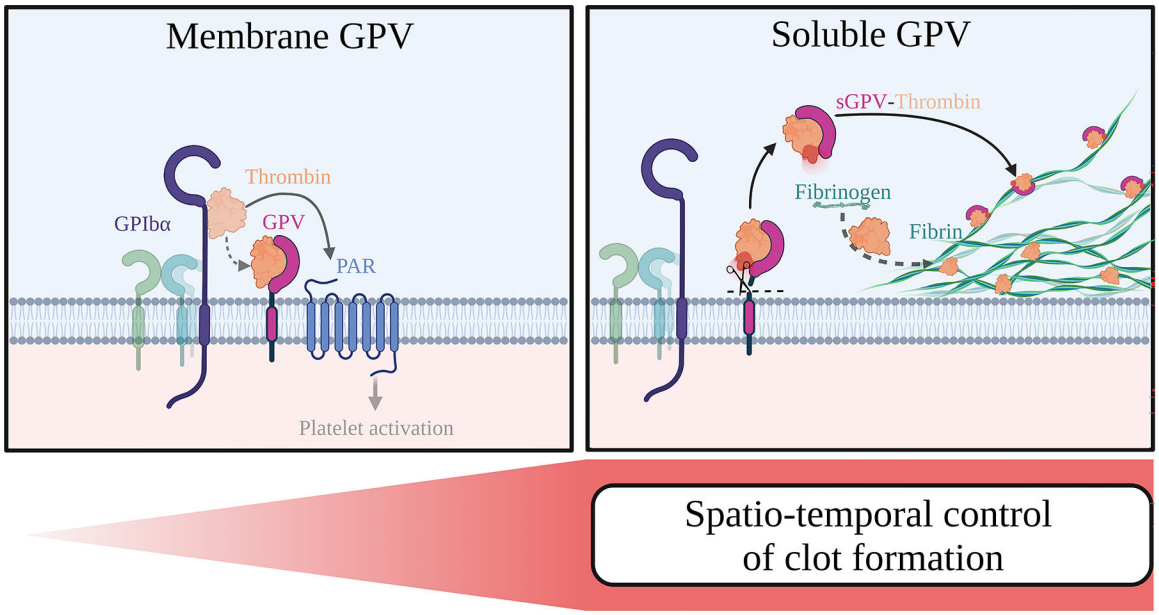

Fig. 6. GPV modulates thrombin-mediated platelet activation and fibrin formation.

On the platelet surface, GPV regulates platelet responsiveness to thrombin by interference with GPIbα-dependent PAR signalling (left panel). Once GPV is cleaved by thrombin, sGPV dampens thrombin activity and fibrin formation, thereby controlling clot formation (right panel). Created with BioRender.